

Stochastic Mirror Descent on Overparameterized Nonlinear Models: Convergence, Implicit Regularization, and Generalization

Navid Azizan¹, Sahin Lale², Babak Hassibi²

¹ Department of Computing and Mathematical Sciences

² Department of Electrical Engineering

California Institute of Technology

{azizan,alale,hassibi}@caltech.edu

Abstract

Most modern learning problems are highly *overparameterized*, meaning that there are many more parameters than the number of training data points, and as a result, the training loss may have infinitely many global minima (parameter vectors that perfectly interpolate the training data). Therefore, it is important to understand which interpolating solutions we converge to, how they depend on the initialization point and the learning algorithm, and whether they lead to different generalization performances. In this paper, we study these questions for the family of stochastic mirror descent (SMD) algorithms, of which the popular stochastic gradient descent (SGD) is a special case. Our contributions are both theoretical and experimental. On the theory side, we show that in the overparameterized *nonlinear* setting, if the initialization is close enough to the manifold of global minima (something that comes for free in the highly overparameterized case), SMD with sufficiently small step size converges to a global minimum that is approximately *the closest one in Bregman divergence*. On the experimental side, our extensive experiments on standard datasets and models, using various initializations, various mirror descents, and various Bregman divergences, consistently confirms that this phenomenon happens in deep learning. Our experiments further indicate that there is a clear difference in the generalization performance of the solutions obtained by different SMD algorithms. Experimenting on a standard image dataset and network architecture with SMD with different kinds of *implicit regularization*, ℓ_1 to encourage sparsity, ℓ_2 yielding SGD, and ℓ_{10} to discourage large components in the parameter vector, consistently and definitively shows that ℓ_{10} -SMD has better generalization performance than SGD, which in turn has better generalization performance than ℓ_1 -SMD. This surprising, and perhaps counter-intuitive, result strongly suggests the importance of a comprehensive study of the role of regularization, and the choice of the best regularizer, to improve the generalization performance of deep networks.

1 Introduction

Deep learning has demonstrably enjoyed a great deal of success in a wide variety of tasks [3, 11, 21, 28, 33, 38, 22]. Despite its tremendous success, the reasons behind the good performance of these methods on unseen data is not fully understood (and, arguably, remains somewhat of a mystery). While the special deep architecture of these models seems to be important to the success of deep learning, the architecture is only part of the story, and it has been now widely recognized that the

optimization algorithms used to train these models, typically stochastic gradient descent (SGD) and its variants, also play a key role in learning parameters that generalize well.

Since these deep models are *highly overparameterized*, they have a lot of capacity, and can fit to virtually any (even random) set of data points [39]. In other words, these highly overparameterized models can “interpolate” the data, so much so that this regime has been called the “interpolating regime” [27]. In fact, on a given dataset, the loss function typically has (infinitely) many *global minima*, which however can have drastically different generalization properties (many of them perform very poorly on the test set). Which minimum among all the possible minima we choose in practice is determined by the initialization and the optimization algorithm that we use for training the model.

Since the loss functions of deep neural networks are non-convex and sometimes even non-smooth, in theory, one may expect the optimization algorithms to get stuck in local minima or saddle points. In practice, however, such simple stochastic descent algorithms almost always reach *zero training error*, i.e., a *global minimum* of the training loss [39, 24]. More remarkably, even in the absence of any explicit regularization, dropout, or early stopping [39], the global minima obtained by these algorithms seem to generalize quite well to unseen data (contrary to many other global minima). It has been also observed that even among different optimization algorithms, i.e., SGD and its variants, there is a discrepancy in the solutions achieved by different algorithms and their generalization capabilities [37]. Therefore, it is important to ask the question

Which global minima do these algorithms converge to?

In this paper, we study the family of stochastic mirror descent (SMD) algorithms, which includes the popular SGD algorithm. For any choice of potential function, there is a corresponding mirror descent algorithm. We show that, for overparameterized nonlinear models, if one initializes close enough to the manifold of parameter vectors that interpolates the data, then the SMD algorithm for any particular potential converges to a global minimum that is approximately ***the closest one to the initialization, in Bregman divergence corresponding to the potential***. Furthermore, in highly overparameterized models, this closeness of the initialization comes for free, something that is occasionally referred to as “the blessing of dimensionality.” For the special case of SGD, this means that it converges to a global minimum which is approximately the closest one to the initialization in the usual Euclidean sense.

We perform extensive systematic experiments on various initializations, various mirror algorithms for the MNIST and CIFAR-10 datasets using the existing off-the-shelf deep neural network architectures, and we measure all the pairwise distances in different Bregman divergences. We found that every single result is exactly consistent with the hypothesis. Indeed, in all our experiments, ***the global minimum achieved by any particular mirror descent algorithm is the closest, among all other global minima obtained by other mirrors and other initializations, to its initialization in the corresponding Bregman divergence***. In particular, the global minimum obtained by SGD from any particular initialization is closest to the initialization in Euclidean sense, both among the global minima obtained by different mirrors and among the global minima obtained by different initializations.

This result further implies that, even in the absence of any explicit regularization, these algorithms perform an *implicit regularization* [30, 26, 15, 13, 5, 36]. In particular, when initialized around zero, SGD acts as an ℓ_2 regularizer. Similarly, by choosing other mirrors, one can obtain different implicit regularizers (such as ℓ_1 or ℓ_∞), which may have different performances on test data. This raises the question

How well do different mirrors perform in practice?

Perhaps, one might expect an ℓ_1 regularizer to perform better, due to the fact that it promotes sparsity, and “pruning” in neural networks is believed to be helpful for generalization. On the other hand, one may expect SGD (ℓ_2 regularizer) to work best among different mirrors, because typical architectures have been tuned for and tailored to SGD. We run experiments with four different mirror descents, i.e., ℓ_1 (sparse), ℓ_2 (SGD), ℓ_3 , and ℓ_{10} (as a surrogate for ℓ_∞), on a standard off-the-shelf deep neural network architecture for CIFAR-10. ***Somewhat counter-intuitively, our results for test errors of different mirrors consistently and definitively show that the ℓ_{10} regularizer performs better than the other mirrors including SGD, while ℓ_1 consistently performs worse.*** This flies in the face of the conventional wisdom that sparser weights (which are obtained by an ℓ_1 regularizer) generalize better, and suggests that ℓ_∞ , which roughly speaking penalizes all the weights uniformly, may be a better regularizer for deep neural networks.

In Section 2, we review the family of mirror descent algorithms and briefly revisit the linear overparameterized case. Section 3 provides our main theoretical results, which are (1) convergence of SMD, under reasonable conditions, to a global minimum, and (2) proximity of the obtained global minimum to the closest point from initialization in Bregman divergence. Our proofs are remarkably simple and are based on a powerful *fundamental identity* that holds for all SMD algorithms in a general setting. We comment on the related work in Section 4. In Section 5, we provide our experimental results, which consists of two parts, (1) testing the theoretical claims about the distances for different mirrors and different initializations, and (2) assessing the generalization properties of different mirrors. The proofs of the theoretical results and more details on the experiments are relegated to the appendix.

2 Background and Warm-Up

2.1 Preliminaries

Let us denote the training dataset by $\{(x_i, y_i) : i = 1, \dots, n\}$, where $x_i \in \mathbb{R}^d$ are the inputs, and $y_i \in \mathbb{R}$ are the labels. The model (which can be linear, a deep neural network, etc.) is defined by the general function $f(x_i, w) = f_i(w)$ with some parameter vector $w \in \mathbb{R}^p$. Since typical deep models have a lot of capacity and are highly overparameterized, we are particularly interested in the overparameterized (so-called interpolating) regime, where $p > n$ (often $p \gg n$). In this case, there are many parameter vectors w that are consistent with the training data points. We denote the set of these parameter vectors by

$$\mathcal{W} = \{w \in \mathbb{R}^p \mid f(x_i, w) = y_i, i = 1, \dots, n\} \tag{1}$$

This a high-dimensional set (e.g. a $(p - n)$ -dimensional manifold) in \mathbb{R}^p and depends only on the training data $\{(x_i, y_i) : i = 1, \dots, n\}$ and the model $f(\cdot, \cdot)$.

The total loss on the training set (empirical risk) can be expressed as $L(w) = \sum_{i=1}^n L_i(w)$, where $L_i(\cdot) = \ell(y_i, f(x_i, w))$ is the loss on the individual data point i , and $\ell(\cdot, \cdot)$ is a differentiable non-negative function, with the property that $\ell(y_i, f(x_i, w)) = 0$ iff $y_i = f(x_i, w)$. Often $\ell(y_i, f(x_i, w)) = \ell(y_i - f(x_i, w))$, with $\ell(\cdot)$ convex and having a global minimum at zero (such as square loss, Huber loss, etc.). In this case, $L(w) = \sum_{i=1}^n \ell(y_i - f(x_i, w))$.

\mathcal{W} is the set of global minima, and every parameter vector w in \mathcal{W} renders the loss on each data point zero, i.e., $L_i(w) = 0 \forall i$. The loss function is often attempted to be minimized by stochastic gradient descent (SGD), which is defined as

$$w_i = w_{i-1} - \eta \nabla L_i(w_{i-1}), \quad i \geq 1 \quad (2)$$

assuming the data is indexed randomly (for $i > n$, one can cycle through the data or select them at random).

2.2 Stochastic Mirror Descent

Stochastic mirror descent (SMD), first introduced by Nemirovski and Yudin [29], is one of the most widely used families of algorithms for stochastic optimization [6, 7, 40], which includes the popular stochastic gradient descent (SGD) as a special case. Consider a strictly convex differentiable function $\psi(\cdot)$, called the *potential function*. Then SMD updates are defined as

$$\nabla \psi(w_i) = \nabla \psi(w_{i-1}) - \eta \nabla L_i(w_{i-1}). \quad (3)$$

Note that, due to the strict convexity of $\psi(\cdot)$, the gradient $\nabla \psi(\cdot)$ defines an invertible map, so the recursion in (3) yields a unique w_i at each iteration, and thus is a well-defined update. Compared to classical SGD, rather than update the weight vector along the direction of the negative gradient, the update is done in the “mirrored” domain determined by the invertible transformation $\nabla \psi(\cdot)$. Mirror descent was originally conceived to exploit the geometrical structure of the problem by choosing an appropriate potential. Note that SMD reduces to SGD when $\psi(w) = \frac{1}{2} \|w\|^2$, since the gradient $\nabla \psi(\cdot)$ is simply the identity map.

Alternatively, the update rule (3) can be expressed as

$$w_i = \arg \min_w \eta w^T \nabla L_i(w_{i-1}) + D_\psi(w, w_{i-1}), \quad (4)$$

where

$$D_\psi(w, w_{i-1}) := \psi(w) - \psi(w_{i-1}) - \nabla \psi(w_{i-1})^T (w - w_{i-1}) \quad (5)$$

is the Bregman divergence with respect to the potential function $\psi(\cdot)$. Note that $D_\psi(\cdot, \cdot)$ is non-negative, convex in its first argument, and that, due to strict convexity, $D_\psi(w, w') = 0$ iff $w = w'$.

Different choices of the potential function $\psi(\cdot)$ yield different optimization algorithms, which will potentially have different implicit biases. A few examples follow.

Gradient Descent. For the potential function $\psi(w) = \frac{1}{2} \|w\|^2$, the Bregman divergence is $D_\psi(w, w') = \frac{1}{2} \|w - w'\|^2$, and the update rule reduces to that of SGD.

Exponentiated Gradient Descent. For $\psi(w) = \sum_j w_j \log w_j$, the Bregman divergence becomes the unnormalized relative entropy (Kullback-Leibler divergence) $D_\psi(w, w') = \sum_j w_j \log \frac{w_j}{w'_j} - \sum_j w_j + \sum_j w'_j$, which corresponds to the exponentiated gradient descent (aka the exponential weights) algorithm [19].

p -norms Algorithm. For any q -norm squared potential function $\psi(w) = \frac{1}{2} \|w\|_q^2$, with $\frac{1}{p} + \frac{1}{q} = 1$, the algorithm will reduce to the so-called p -norms algorithm [12, 10].

Sparse Mirror Descent. For $\psi(w) = \|w\|_{1+\epsilon}^{1+\epsilon}$, the algorithm reduces to sparse mirror descent, which is used in compressed sensing [5, 4].

2.3 Overparameterized Linear Models

Overparameterized (or underdetermined) linear models have been recently studied in many papers due to their simplicity, and there are interesting insights than one can obtain from them. In this case, the model is $f(x_i, w) = x_i^T w$, the set of global minima is $\mathcal{W} = \{w \mid y_i = x_i^T w, i = 1, \dots, n\}$, and the loss is $L_i(w) = \ell(y_i - x_i^T w)$. The following result characterizes the solution that SMD converges to, in the linear overparameterized setting [5, 13].

Proposition 1. *Consider a linear overparameterized model. For sufficiently small step size, i.e., for any $\eta > 0$ for which $\psi(\cdot) - \eta L_i(\cdot)$ is convex, and for any initialization w_0 , the SMD iterates converge to*

$$w_\infty = \arg \min_{w \in \mathcal{W}} D_\psi(w, w_0).$$

Note that the step size condition, i.e., the convexity of $\psi(\cdot) - \eta L_i(\cdot)$, depends on both the loss and the potential function. For the case of SGD, $\psi(w) = \frac{1}{2} \|w\|^2$, and the condition reduces to $\eta \leq \frac{1}{\|x_i\|^2}$. In that case, $D_\psi(w, w_0)$ is simply $\frac{1}{2} \|w - w_0\|^2$.

Corollary 2. *In particular, for the initialization $w_0 = \arg \min_{w \in \mathbb{R}^p} \psi(w)$, under the conditions of Proposition 1, the SMD iterates converge to*

$$w_\infty = \arg \min_{w \in \mathcal{W}} \psi(w). \tag{6}$$

This means that running SMD for a linear model with the aforementioned w_0 , without any explicit regularization, results in a solution that has the smallest potential $\psi(\cdot)$ among all solutions, i.e., SMD implicitly regularizes the solution with $\psi(\cdot)$. For example, SGD initialized around zero acts as an ℓ_2 regularizer. We will show that these results continue to hold for highly overparameterized nonlinear models in an approximate sense.

3 Theoretical Results

In this section, we provide our main theoretical results. In particular, we show that for highly overparameterized nonlinear models, if initialized close enough to the set \mathcal{W} , (1) SMD converges to a global minimum, (2) the global minimum obtained by SMD is approximately the closest one to the initialization in Bregman divergence corresponding to the potential.

3.1 Convergence of Stochastic Mirror Descent

Let us define

$$D_{L_i}(w, w') := L_i(w) - L_i(w') - \nabla L_i(w')^T (w - w'), \tag{7}$$

which is defined in a similar way to a Bregman divergence for the loss function. The difference though is that, unlike the potential function of the Bregman divergence, the loss function $L_i(\cdot) = \ell(y_i - f(x_i, \cdot))$ need not be convex (even when $\ell(\cdot)$ is) due to the nonlinearity of $f(\cdot, \cdot)$. As a result, $D_{L_i}(w, w')$ is not necessarily non-negative.

It has been argued in several recent papers that in highly overparameterized neural networks, any random initialization w_0 is close to \mathcal{W} , with high probability [25, 9, 5, 2] (see also the discussion in Section A.4 of the supplementary material). Therefore, it is reasonable to make the following assumption about the initialization.

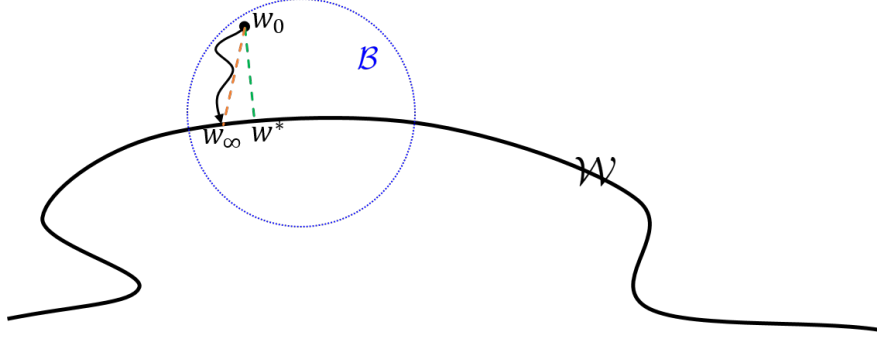


Figure 1: An illustration of the parameter space. \mathcal{W} represents the set of global minima, w_0 is the initialization, \mathcal{B} is the local neighborhood, w^* and the closest global minimum to w_0 (in Bregman divergence), and w_∞ is the minimum that SMD converges to.

Assumption 1. Denote the initial point by w_0 . There exists $w \in \mathcal{W}$ and a region $\mathcal{B} = \{w' \in \mathbb{R}^p \mid D_\psi(w, w') \leq \epsilon\}$ containing w_0 , such that $D_{L_i}(w, w') \geq 0, i = 1, \dots, n$, for all $w' \in \mathcal{B}$.

This assumption states that, while L_i certainly need not be convex, since w is a minimizer of $L_i(\cdot)$, the initial point is close to \mathcal{W} so that $D_{L_i}(w, w_0) \geq 0$ (see Fig. 2 for an illustration).

Our second assumption states that in this local region, the first and second derivatives of the model are bounded.

Assumption 2. Consider the region \mathcal{B} in Assumption 1. $f_i(\cdot)$ have bounded gradient and Hessian on the convex hull of \mathcal{B} , i.e., $\|\nabla f_i(w')\| \leq \gamma$, and $\alpha \leq \lambda_{\min}(H_{f_i}(w')) \leq \lambda_{\max}(H_{f_i}(w')) \leq \beta, i = 1, \dots, n$, for all $w' \in \text{conv } \mathcal{B}$.

This is again a mild assumption, which is assumed in other related works such as [31] as well. The following theorem states that under Assumption 1, SMD converges to a global minimum.

Theorem 3. Consider the set of interpolating parameters $\mathcal{W} = \{w \in \mathbb{R}^p \mid f(x_i, w) = y_i, i = 1, \dots, n\}$, and the SMD iterates given in (3), where every data point is revisited after some steps. Under Assumption 1, for sufficiently small step size, i.e., for any $\eta > 0$ for which $\psi(\cdot) - \eta L_i(\cdot)$ is strictly convex for all i , the following holds.

1. All the iterates $\{w_i\}$ remain in \mathcal{B} .
2. The iterates converge (to w_∞).
3. $w_\infty \in \mathcal{W}$.

Note that, while convergence (to some point) with decaying step size is almost trivial, this result establishes convergence to the solution set with *fixed* step size. Furthermore, the convergence is *deterministic*, and is not in expectation or with high probability. For example, this result also applies to the case where we cycle through the data deterministically.

We should also remark that the choice of distance in the definition of the “ball” \mathcal{B} was important to be the Bregman divergence with respect to ψ and in that particular order. In fact, one cannot

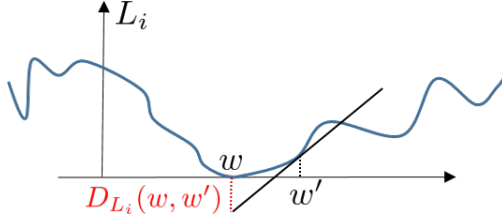


Figure 2: An illustration of $D_{L_i}(w, w') \geq 0$ in a local region in Assumption 1.

guarantee that SMD gets closer to (i.e. does not get farther from) w at every step in the usual Euclidean sense. At some steps, it may get farther from w in other senses, while getting closer in $D_\psi(w, \cdot)$.

Denote the global minimum that is closest to the initialization in Bregman divergence by w^* , i.e.,

$$w^* = \arg \min_{w \in \mathcal{W}} D_\psi(w, w_0). \quad (8)$$

Recall that in the linear case, this was what SMD converges to. We show that in the nonlinear case, under Assumptions 1 and 2, SMD converges to a point w_∞ which is “very close” to w^* .

Theorem 4. *Define $w^* = \arg \min_{w \in \mathcal{W}} D_\psi(w, w_0)$. Under the assumptions of Theorem 3, and Assumption 2, the following holds.*

1. $D_\psi(w_\infty, w_0) = D_\psi(w^*, w_0) + o(\epsilon)$
2. $D_\psi(w^*, w_\infty) = o(\epsilon)$

In other words, if we start with an initialization that is $O(\epsilon)$ away from \mathcal{W} (in Bregman divergence), we converge to a point w_∞ that is $o(\epsilon)$ away from the w^* , the closest point on \mathcal{W} .

Corollary 5. *For the initialization $w_0 = \arg \min_{w \in \mathbb{R}^p} \psi(w)$, under the conditions of Theorem 4, $w^* = \arg \min_{w \in \mathcal{W}} \psi(w)$ and the following holds.*

1. $\psi(w_\infty) = \psi(w^*) + o(\epsilon)$
2. $D_\psi(w^*, w_\infty) = o(\epsilon)$

3.2 Proof Technique: Fundamental Identity of SMD

The main tool used for the proofs is a fundamental identity that holds for SMD in a very general setting.

Lemma 6. *For any model $f(\cdot, \cdot)$, any differentiable loss $\ell(\cdot)$, any parameter $w \in \mathcal{W}$, and any step size $\eta > 0$, the following relation holds for the SMD iterates $\{w_i\}$*

$$D_\psi(w, w_{i-1}) = D_\psi(w, w_i) + D_{\psi-\eta L_i}(w_i, w_{i-1}) + \eta L_i(w_i) + \eta D_{L_i}(w, w_{i-1}), \quad (9)$$

for all $i \geq 1$.

This identity allows one to prove the results in a remarkably simple and direct way. Due to space limitations, the proofs are relegated to the supplementary material.

The ideas behind this identity are related to H_∞ estimation theory [17, 34], which was originally developed in the 1990’s in the context of robust control theory. In fact, it has connections to the minimax optimality of SGD, which was shown by [16] for linear models, and recently extended to nonlinear models and general mirrors by [5].

4 Related Work

There have been many efforts in the past few years to study deep learning from an optimization perspective, e.g., [1, 8, 32, 2, 31, 5, 27, 9, 25]. While it is not possible to review all the contributions here, we comment on the ones that are most closely related to our results. We highlight the distinctions between our results and those.

Many recent papers have studied the so-called “overparameterized” setting, or the “interpolating” regime, which is common in deep learning [31, 2, 35, 27]. All these results, similar to our work, have assumptions for being close to the solution space (global minima), which is perhaps reasonable in highly overparameterized models, as we also argued in Section A.4 of the supplementary material. However, most of these results are limited to (S)GD and do not generalize to more general mirrors.

Furthermore, even for the case of SGD, our results are stronger than those in the literature, in the sense that not only do we show convergence to a global minimum, but we also show that w_∞ and w^* are close. In fact, [31] showed that for SGD, $\|w - w_\infty\|$ is close to (i.e. bounded by a constant factor of) $\|w - w^*\|$. Our Theorem 4 states that not only are these two distances close, but w_∞ and w^* are also actually close ($\|w_\infty - w^*\|^2 = o(\epsilon)$), something that could not be inferred from the previous work.

As mentioned before, there have been a number of results on characterizing the implicit regularization properties of different algorithms in different contexts [30, 26, 15, 13, 36, 14, 5]. The closest ones to our results, which concern mirror descent, are the works of [13, 5]. The authors in [13] consider *linear* overparameterized models, and show that *if* SMD happens to converge to a global minimum, then that global minimum should be the one that is closest in Bregman divergence to the initialization, which can be shown by writing the KKT conditions. In fact, they do not provide any conditions for convergence and whether it converges with a fixed step size or not. In the authors’ earlier work [5], the condition on the step size for which SMD converges to the aforementioned global minimum was derived, for linear models. Our results in this paper are for *nonlinear* models, and we show that, under the specified conditions on the step size, these algorithms with a *fixed* step size converge to the mentioned global minimum, which had not been shown in any of the previous work. Furthermore, assuming every data point is revisited again after some steps, the convergence we establish is *deterministic*, and not in expectation or with high probability.

5 Experimental Results

In this section, we provide our experimental results, which consist of two main parts. In the first part, we evaluate the theoretical claims by running systematic experiments for different initializations and different mirrors, and evaluating the distances between the global minima achieved and the initializations, in different Bregman divergences. In the second part, we assess the generalization

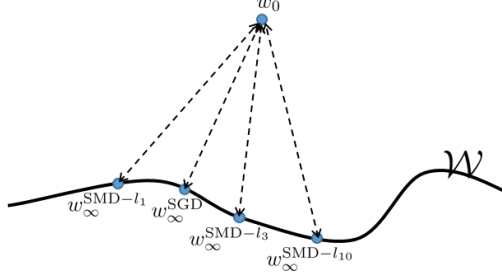


Figure 3: An illustration of the experiments in Table 1

Table 1: Fixed Initialization. Distances from final points (global minima) obtained by different algorithms (columns) from the same initialization (Fig.3), measured in different Bregman divergences (rows). **First Row:** The closest point to w_0 in ℓ_1 Bregman divergence, among the four final points, is exactly the one obtained by SMD with 1-norm potential. **Second Row:** The closest point to w_0 in ℓ_2 Bregman divergence (Euclidean distance), among the four final points, is exactly the one obtained by SGD. **Third Row:** The closest point to w_0 in ℓ_3 Bregman divergence, among the four final points, is exactly the one obtained by SMD with 3-norm potential. **Fourth Row:** The closest point to w_0 in ℓ_{10} Bregman divergence, among the four final points, is exactly the one obtained by SMD with 10-norm potential.

	SMD 1-norm	SMD 2-norm (SGD)	SMD 3-norm	SMD 10-norm
1-norm BD	141	9.19×10^3	4.1×10^4	2.34×10^5
2-norm BD	3.15×10^3	562	1.24×10^3	6.89×10^3
3-norm BD	4.31×10^4	107	53.5	1.85×10^2
10-norm BD	6.83×10^{13}	972	7.91×10^{-5}	2.72×10^{-8}

error of different mirrors, which correspond to different regularizers, in order to understand which regularizer performs better.

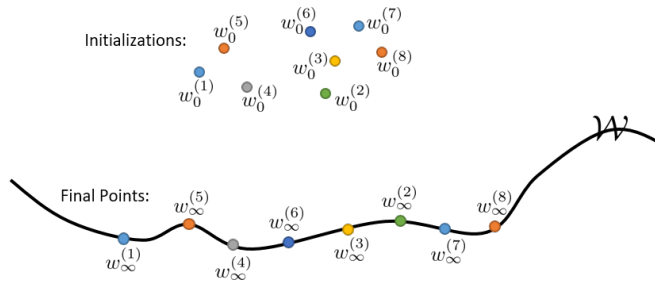


Figure 4: An illustration of the experiments in Table 2

Table 2: Fixed Mirror: SGD. Pairwise distances between different initial points and the final points obtained from them by SGD (Fig 4). **Row i** : The closest final point to the initial point i , among all the eight final points, is exactly the one obtained by the algorithm from initialization i .

	Final 1	Final 2	Final 3	Final 4	Final 5	Final 6	Final 7	Final 8
Initial 1	6×10^2	2.9×10^3	2.8×10^3					
Initial 2	2.8×10^3	6.1×10^2	2.8×10^3					
Initial 3	2.8×10^3	2.9×10^3	5.6×10^2	2.8×10^3				
Initial 4	2.8×10^3	2.9×10^3	2.8×10^3	5.9×10^2	2.8×10^3	2.8×10^3	2.8×10^3	2.8×10^3
Initial 5	2.8×10^3	2.9×10^3	2.8×10^3	2.8×10^3	5.7×10^2	2.8×10^3	2.8×10^3	2.8×10^3
Initial 6	2.8×10^3	2.9×10^3	2.8×10^3	2.8×10^3	2.8×10^3	5.6×10^2	2.8×10^3	2.8×10^3
Initial 7	2.8×10^3	2.9×10^3	2.8×10^3	2.8×10^3	2.8×10^3	2.8×10^3	6×10^2	2.8×10^3
Initial 8	2.8×10^3	2.9×10^3	2.8×10^3	5.8×10^2				

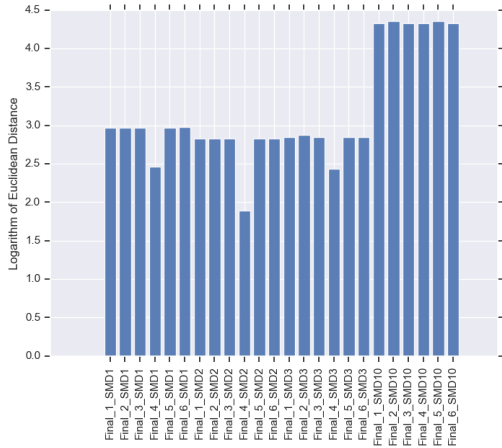
5.1 Do SMDs Converge to the Closest Point in Bregman Divergence?

While accessing all the points on \mathcal{W} and finding the closest one is impossible, we design systematic experiments to test this claim. We run experiments on some standard deep learning problems, namely, a standard CNN on MNIST [23] and the ResNet-18 [18] on CIFAR-10 [20]. We train the models from different initializations, and with different mirror descents from each particular initialization, until we reach 100% training accuracy, i.e., a point on \mathcal{W} . We randomly initialize the parameters of the networks around zero. We choose 6 independent initializations for the CNN, and 8 for ResNet-18, and for each initialization, we run different SMD algorithms with the following four potential functions: (a) ℓ_1 norm, (b) ℓ_2 norm (which is SGD), (c) ℓ_3 norm, (d) ℓ_{10} norm (as a surrogate for ℓ_∞). See Appendix B for more details on the experiments.

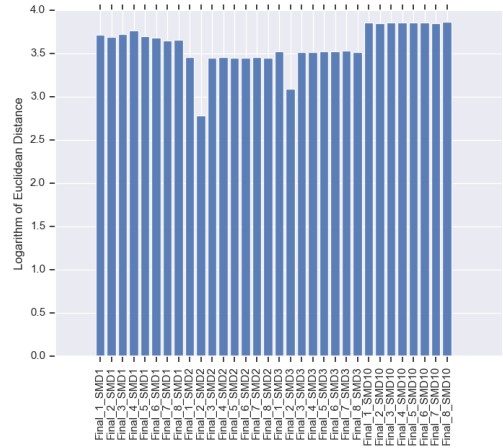
We measure the distances between the initializations and the global minima obtained from different mirrors and different initializations, in different Bregman divergences. Table 1, and Table 2 show some examples among different mirrors and different initializations, respectively. Fig. 5 shows the distances between a particular initial point and all the final points obtained from different initializations and different mirrors (the distances are often orders of magnitude different, so we show them in logarithmic scale). The global minimum achieved by any mirror from any initialization is the closest in the correct Bregman divergence, among all mirrors, among all initializations, and among both. This trend is very consistent among all our experiments, which can be found in Appendix B.

5.2 Distribution of the Weights of the Network

One may be curious to see how the final weights obtained by these different mirrors look like, and whether, for example, mirror descent corresponding to the ℓ_1 -norm potential induces sparsity. Fig 6 shows the histogram of the absolute value of the weights for different SMDs. The histogram of the ℓ_1 -SMD has more weights at and close to zero, which again confirms that it induces sparsity. However, as will be shown in the next section, this is not necessarily good for generalization. The histogram of the ℓ_2 -SMD (SGD) looks almost identical to the histogram of the initialization, whereas the ℓ_3 and ℓ_{10} histograms are shifted to the right, so much so that almost all weights in the ℓ_{10} solution are non-zero. See Appendix B for individual histograms and more details.



MNIST. SGD Starting from Initial 4



CIFAR-10. SGD Starting from Initial 2

Figure 5: Distances between a particular initial point and all the final points obtained by both different initializations and different mirrors. The smallest distance, among all initializations and all mirrors, corresponds exactly to the final point obtained from that initial point by SGD. This trend is observed consistently for all other mirror descents and all initializations (see the results in Tables 8 and 9 in the appendix).

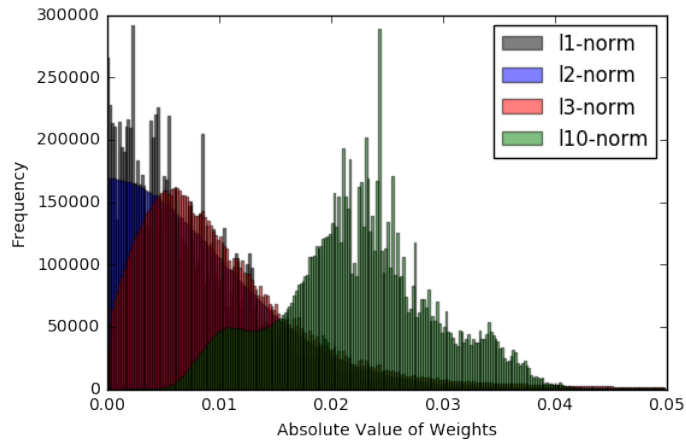


Figure 6: Histogram of the absolute value of the final weights in the network for different SMD algorithm with different potentials. Note that each of the four histograms corresponds to an 11×10^6 -dimensional weight vector that perfectly interpolates the data. Even though the weights remain quite small, the histograms are drastically different. ℓ_1 -SMD induces sparsity on the weights, as expected. SGD does not seem to change the distribution of the weights significantly. ℓ_3 -SMD starts to reduce the sparsity, and ℓ_{10} shifts the distribution of the weights significantly, so much so that almost all the weights are non-zero.

5.3 Generalization Errors of Different Mirrors

We compare the performance of the SMD algorithms discussed before on the test set. For MNIST, perhaps not surprisingly, all the four SMD algorithms achieve around 99% or higher accuracy. For CIFAR-10, however, there is a significant difference between the test errors of different mirrors/regularizers on the same architecture. Fig. 7 shows the test accuracies of different algorithms with eight random initializations around zero, as discussed before. Counter-intuitively, ℓ_{10} performs consistently best, while ℓ_1 performs consistently worse. This result suggests the importance of a comprehensive study of the role of regularization, and the choice of the best regularizer, to improve the generalization performance of deep neural networks.

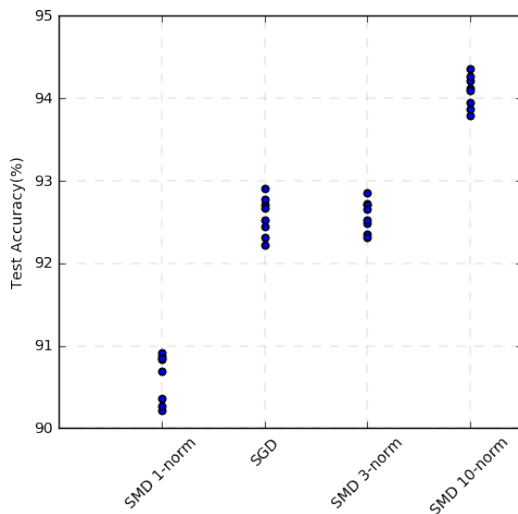


Figure 7: Generalization performance of different SMD algorithms on the CIFAR-10 dataset using ResNet-18. ℓ_{10} performs consistently better, while ℓ_1 performs consistently worse.

References

- [1] Alessandro Achille and Stefano Soatto. On the emergence of invariance and disentangling in deep representations. *arXiv preprint arXiv:1706.01350*, 2017.
- [2] Zeyuan Allen-Zhu, Yuanzhi Li, and Zhao Song. A convergence theory for deep learning via over-parameterization. In *Proceedings of the 36th International Conference on Machine Learning*. PMLR, 2019.
- [3] Dario Amodei, Sundaram Ananthanarayanan, Rishita Anubhai, Jingliang Bai, Eric Battenberg, Carl Case, Jared Casper, Bryan Catanzaro, Qiang Cheng, Guoliang Chen, et al. Deep speech 2: End-to-end speech recognition in english and mandarin. In *International Conference on Machine Learning*, pages 173–182, 2016.

- [4] Navid Azizan and Babak Hassibi. A characterization of stochastic mirror descent algorithms and their convergence properties. In *IEEE International Conference on Acoustics, Speech and Signal Processing (ICASSP)*, 2019.
- [5] Navid Azizan and Babak Hassibi. Stochastic gradient/mirror descent: Minimax optimality and implicit regularization. In *International Conference on Learning Representations (ICLR)*, 2019.
- [6] Amir Beck and Marc Teboulle. Mirror descent and nonlinear projected subgradient methods for convex optimization. *Operations Research Letters*, 31(3):167–175, 2003.
- [7] Nicolo Cesa-Bianchi, Pierre Gaillard, Gábor Lugosi, and Gilles Stoltz. Mirror descent meets fixed share (and feels no regret). In *Advances in Neural Information Processing Systems*, pages 980–988, 2012.
- [8] Pratik Chaudhari and Stefano Soatto. Stochastic gradient descent performs variational inference, converges to limit cycles for deep networks. In *International Conference on Learning Representations*, 2018.
- [9] Simon S Du, Jason D Lee, Haochuan Li, Liwei Wang, and Xiyu Zhai. Gradient descent finds global minima of deep neural networks. *arXiv preprint arXiv:1811.03804*, 2018.
- [10] Claudio Gentile. The robustness of the p-norm algorithms. *Machine Learning*, 53(3):265–299, 2003.
- [11] Alex Graves, Abdel-rahman Mohamed, and Geoffrey Hinton. Speech recognition with deep recurrent neural networks. In *2013 IEEE international conference on acoustics, speech and signal processing*, pages 6645–6649. IEEE, 2013.
- [12] Adam J Grove, Nick Littlestone, and Dale Schuurmans. General convergence results for linear discriminant updates. *Machine Learning*, 43(3):173–210, 2001.
- [13] Suriya Gunasekar, Jason Lee, Daniel Soudry, and Nathan Srebro. Characterizing implicit bias in terms of optimization geometry. In *International Conference on Machine Learning*, pages 1827–1836, 2018.
- [14] Suriya Gunasekar, Jason Lee, Daniel Soudry, and Nathan Srebro. Implicit bias of gradient descent on linear convolutional networks. *arXiv preprint arXiv:1806.00468*, 2018.
- [15] Suriya Gunasekar, Blake E Woodworth, Srinadh Bhojanapalli, Behnam Neyshabur, and Nati Srebro. Implicit regularization in matrix factorization. In *Advances in Neural Information Processing Systems*, pages 6152–6160, 2017.
- [16] Babak Hassibi, Ali H. Sayed, and Thomas Kailath. Hoo optimality criteria for LMS and backpropagation. In *Advances in Neural Information Processing Systems 6*, pages 351–358. 1994.
- [17] Babak Hassibi, Ali H Sayed, and Thomas Kailath. *Indefinite-Quadratic Estimation and Control: A Unified Approach to H2 and H-infinity Theories*, volume 16. SIAM, 1999.

- [18] Kaiming He, Xiangyu Zhang, Shaoqing Ren, and Jian Sun. Deep residual learning for image recognition. In *Proceedings of the IEEE conference on computer vision and pattern recognition*, pages 770–778, 2016.
- [19] Jyrki Kivinen and Manfred K Warmuth. Exponentiated gradient versus gradient descent for linear predictors. *Information and Computation*, 132(1):1–63, 1997.
- [20] Alex Krizhevsky and Geoffrey Hinton. Learning multiple layers of features from tiny images. Technical report, Citeseer, 2009.
- [21] Alex Krizhevsky, Ilya Sutskever, and Geoffrey E Hinton. Imagenet classification with deep convolutional neural networks. In *Advances in Neural Information Processing Systems*, pages 1097–1105, 2012.
- [22] Yann LeCun, Yoshua Bengio, and Geoffrey Hinton. Deep learning. *Nature*, 521(7553):436, 2015.
- [23] Yann LeCun, Léon Bottou, Yoshua Bengio, and Patrick Haffner. Gradient-based learning applied to document recognition. *Proceedings of the IEEE*, 86(11):2278–2324, 1998.
- [24] Jason D Lee, Max Simchowitz, Michael I Jordan, and Benjamin Recht. Gradient descent only converges to minimizers. In *Conference on Learning Theory*, pages 1246–1257, 2016.
- [25] Yuanzhi Li and Yingyu Liang. Learning overparameterized neural networks via stochastic gradient descent on structured data. In *Advances in Neural Information Processing Systems*, pages 8157–8166, 2018.
- [26] Cong Ma, Kaizheng Wang, Yuejie Chi, and Yuxin Chen. Implicit regularization in nonconvex statistical estimation: Gradient descent converges linearly for phase retrieval, matrix completion and blind deconvolution. *arXiv preprint arXiv:1711.10467*, 2017.
- [27] Siyuan Ma, Raef Bassily, and Mikhail Belkin. The power of interpolation: Understanding the effectiveness of SGD in modern over-parametrized learning. In *Proceedings of the 35th International Conference on Machine Learning*, volume 80, pages 3325–3334. PMLR, 2018.
- [28] Volodymyr Mnih, Koray Kavukcuoglu, David Silver, Andrei A Rusu, Joel Veness, Marc G Bellemare, Alex Graves, Martin Riedmiller, Andreas K Fidjeland, Georg Ostrovski, et al. Human-level control through deep reinforcement learning. *Nature*, 518(7540):529, 2015.
- [29] Arkadii Nemirovski and David Borisovich Yudin. Problem complexity and method efficiency in optimization. 1983.
- [30] Behnam Neyshabur, Ryota Tomioka, Ruslan Salakhutdinov, and Nathan Srebro. Geometry of optimization and implicit regularization in deep learning. *arXiv preprint arXiv:1705.03071*, 2017.
- [31] Samet Oymak and Mahdi Soltanolkotabi. Overparameterized nonlinear learning: Gradient descent takes the shortest path? In *Proceedings of the 36th International Conference on Machine Learning*. PMLR, 2019.
- [32] Ravid Shwartz-Ziv and Naftali Tishby. Opening the black box of deep neural networks via information. *arXiv preprint arXiv:1703.00810*, 2017.

- [33] David Silver, Aja Huang, Chris J Maddison, Arthur Guez, Laurent Sifre, George Van Den Driessche, Julian Schrittwieser, Ioannis Antonoglou, Veda Panneershelvam, Marc Lanctot, et al. Mastering the game of go with deep neural networks and tree search. *Nature*, 529(7587):484–489, 2016.
- [34] Dan Simon. *Optimal state estimation: Kalman, H infinity, and nonlinear approaches*. John Wiley & Sons, 2006.
- [35] Mahdi Soltanolkotabi, Adel Javanmard, and Jason D Lee. Theoretical insights into the optimization landscape of over-parameterized shallow neural networks. *arXiv preprint arXiv:1707.04926*, 2017.
- [36] Daniel Soudry, Elad Hoffer, Mor Shpigel Nacson, Suriya Gunasekar, and Nathan Srebro. The implicit bias of gradient descent on separable data. *arXiv preprint arXiv:1710.10345*, 2017.
- [37] Ashia C Wilson, Rebecca Roelofs, Mitchell Stern, Nati Srebro, and Benjamin Recht. The marginal value of adaptive gradient methods in machine learning. In *Advances in Neural Information Processing Systems*, pages 4151–4161, 2017.
- [38] Yonghui Wu, Mike Schuster, Zhifeng Chen, Quoc V Le, Mohammad Norouzi, Wolfgang Macherey, Maxim Krikun, Yuan Cao, Qin Gao, Klaus Macherey, et al. Google’s neural machine translation system: Bridging the gap between human and machine translation. *arXiv preprint arXiv:1609.08144*, 2016.
- [39] Chiyuan Zhang, Samy Bengio, Moritz Hardt, Benjamin Recht, and Oriol Vinyals. Understanding deep learning requires rethinking generalization. *arXiv preprint arXiv:1611.03530*, 2016.
- [40] Zhengyuan Zhou, Panayotis Mertikopoulos, Nicholas Bambos, Stephen Boyd, and Peter W Glynn. Stochastic mirror descent in variationally coherent optimization problems. In *Advances in Neural Information Processing Systems*, pages 7043–7052, 2017.

Supplementary Material

A Proofs of the Theoretical Results

In this section, we prove the main theoretical results. The proofs are based on a fundamental identity about the iterates of SMD, which holds for all mirrors and all overparameterized (even nonlinear) models (Lemma 6). We first prove this identity, and then use it to prove the convergence and implicit regularization results.

A.1 Fundamental Identity of SMD

Let us prove the fundamental identity.

Lemma 6. *For any model $f(\cdot, \cdot)$, any differentiable loss $\ell(\cdot)$, any parameter $w \in \mathcal{W}$, and any step size $\eta > 0$, the following relation holds for the SMD iterates $\{w_i\}$*

$$D_\psi(w, w_{i-1}) = D_\psi(w, w_i) + D_{\psi-\eta L_i}(w_i, w_{i-1}) + \eta L_i(w_i) + \eta D_{L_i}(w, w_{i-1}), \quad (9)$$

for all $i \geq 1$.

Proof of Lemma 6. Let us start by expanding the Bregman divergence $D_\psi(w, w_i)$ based on its definition

$$D_\psi(w, w_i) = \psi(w) - \psi(w_i) - \nabla\psi(w_i)^T(w - w_i).$$

By plugging the SMD update rule $\nabla\psi(w_i) = \nabla\psi(w_{i-1}) - \eta\nabla L_i(w_{i-1})$ into this, we can write it as

$$D_\psi(w, w_i) = \psi(w) - \psi(w_i) - \nabla\psi(w_{i-1})^T(w - w_i) + \eta\nabla L_i(w_{i-1})^T(w - w_i). \quad (10)$$

Using the definition of Bregman divergence for (w, w_{i-1}) and (w_i, w_{i-1}) , i.e., $D_\psi(w, w_{i-1}) = \psi(w) - \psi(w_{i-1}) - \nabla\psi(w_{i-1})^T(w - w_{i-1})$ and $D_\psi(w_i, w_{i-1}) = \psi(w_i) - \psi(w_{i-1}) - \nabla\psi(w_{i-1})^T(w_i - w_{i-1})$, we can express this as

$$\begin{aligned} D_\psi(w, w_i) &= D_\psi(w, w_{i-1}) + \psi(w_{i-1}) + \nabla\psi(w_{i-1})^T(w - w_{i-1}) - \psi(w_i) \\ &\quad - \nabla\psi(w_{i-1})^T(w - w_i) + \eta\nabla L_i(w_{i-1})^T(w - w_i) \end{aligned} \quad (11)$$

$$\begin{aligned} &= D_\psi(w, w_{i-1}) + \psi(w_{i-1}) - \psi(w_i) + \nabla\psi(w_{i-1})^T(w_i - w_{i-1}) \\ &\quad + \eta\nabla L_i(w_{i-1})^T(w - w_i) \end{aligned} \quad (12)$$

$$= D_\psi(w, w_{i-1}) - D_\psi(w_i, w_{i-1}) + \eta\nabla L_i(w_{i-1})^T(w - w_i). \quad (13)$$

Expanding the last term using $w - w_i = (w - w_{i-1}) - (w_i - w_{i-1})$, and following the definition of $D_{L_i}(\cdot, \cdot)$ from (7) for (w, w_{i-1}) and (w_i, w_{i-1}) , we have

$$\begin{aligned} D_\psi(w, w_i) &= D_\psi(w, w_{i-1}) - D_\psi(w_i, w_{i-1}) + \eta\nabla L_i(w_{i-1})^T(w - w_{i-1}) \\ &\quad - \eta\nabla L_i(w_{i-1})^T(w_i - w_{i-1}) \end{aligned} \quad (14)$$

$$\begin{aligned} &= D_\psi(w, w_{i-1}) - D_\psi(w_i, w_{i-1}) + \eta(L_i(w) - L_i(w_{i-1}) - D_{L_i}(w, w_{i-1})) \\ &\quad - \eta(L_i(w_i) - L_i(w_{i-1}) - D_{L_i}(w_i, w_{i-1})) \end{aligned} \quad (15)$$

$$\begin{aligned} &= D_\psi(w, w_{i-1}) - D_\psi(w_i, w_{i-1}) + \eta(L_i(w) - D_{L_i}(w, w_{i-1})) \\ &\quad - \eta(L_i(w_i) - D_{L_i}(w_i, w_{i-1})) \end{aligned} \quad (16)$$

Note that for all $w \in \mathcal{W}$, we have $L_i(w) = 0$. Therefore, for all $w \in \mathcal{W}$

$$D_\psi(w, w_i) = D_\psi(w, w_{i-1}) - D_\psi(w_i, w_{i-1}) - \eta D_{L_i}(w, w_{i-1}) - \eta L_i(w_i) + \eta D_{L_i}(w_i, w_{i-1}). \quad (17)$$

Combining the second and the last terms in the right-hand side leads to

$$D_\psi(w, w_i) = D_\psi(w, w_{i-1}) - D_{\psi-\eta L_i}(w_i, w_{i-1}) - \eta D_{L_i}(w, w_{i-1}) - \eta L_i(w_i), \quad (18)$$

for all $w \in \mathcal{W}$, which concludes the proof. \square

A.2 Convergence of SMD to the Interpolating Set

Now that we have proved Lemma 6, we can use it to prove our main results, in a remarkably simple fashion. Let us first prove the convergence of SMD to the set of solutions.

Assumption 1. *Denote the initial point by w_0 . There exists $w \in \mathcal{W}$ and a region $\mathcal{B} = \{w' \in \mathbb{R}^p \mid D_\psi(w, w') \leq \epsilon\}$ containing w_0 , such that $D_{L_i}(w, w') \geq 0, i = 1, \dots, n$, for all $w' \in \mathcal{B}$.*

Theorem 3. *Consider the set of interpolating parameters $\mathcal{W} = \{w \in \mathbb{R}^p \mid f(x_i, w) = y_i, i = 1, \dots, n\}$, and the SMD iterates given in (3), where every data point is revisited after some steps. Under Assumption 1, for sufficiently small step size, i.e., for any $\eta > 0$ for which $\psi(\cdot) - \eta L_i(\cdot)$ is strictly convex for all i , the following holds.*

1. All the iterates $\{w_i\}$ remain in \mathcal{B} .
2. The iterates converge (to w_∞).
3. $w_\infty \in \mathcal{W}$.

Proof of Theorem 3. First we show that all the iterates will remain in \mathcal{B} . Recall the identity of SMD from Lemma 6:

$$D_\psi(w, w_{i-1}) = D_\psi(w, w_i) + D_{\psi-\eta L_i}(w_i, w_{i-1}) + \eta L_i(w_i) + \eta D_{L_i}(w, w_{i-1}) \quad (9)$$

which holds for all $w \in \mathcal{W}$. If w_{i-1} is in the region \mathcal{B} , we know that the last term $D_{L_i}(w, w_{i-1})$ is non-negative. Furthermore, if the step size is small enough that $\psi(\cdot) - \eta L_i(\cdot)$ is strictly convex, the second term $D_{\psi-\eta L_i}(w_i, w_{i-1})$ is a Bregman divergence and is non-negative. Since the loss is non-negative, $\eta L_i(w_i)$ is always non-negative. As a result, we have

$$D_\psi(w, w_{i-1}) \geq D_\psi(w, w_i), \quad (19)$$

This implies that $D_\psi(w, w_i) \leq \epsilon$, which means w_i is in \mathcal{B} too. Since w_0 is in \mathcal{B} , w_1 will be in \mathcal{B} , and therefore, w_2 will be in \mathcal{B} , and similarly all the iterates will remain in \mathcal{B} .

Next, we prove that the iterates converge and $w_\infty \in \mathcal{W}$. If we sum up identity (9) for all $i = 1, \dots, T$, the first terms on the right- and left-hand side cancel each other telescopically, and we have

$$D_\psi(w, w_0) = D_\psi(w, w_T) + \sum_{i=1}^T [D_{\psi-\eta L_i}(w_i, w_{i-1}) + \eta L_i(w_i) + \eta D_{L_i}(w, w_{i-1})]. \quad (20)$$

Since $D_\psi(w, w_T) \geq 0$, we have $\sum_{i=1}^T [D_{\psi-\eta L_i}(w_i, w_{i-1}) + \eta L_i(w_i) + \eta D_{L_i}(w, w_{i-1})] \leq D_\psi(w, w_0)$. If we take $T \rightarrow \infty$, the sum still has to remain bounded, i.e.,

$$\sum_{i=1}^{\infty} [D_{\psi-\eta L_i}(w_i, w_{i-1}) + \eta L_i(w_i) + \eta D_{L_i}(w, w_{i-1})] \leq D_\psi(w, w_0). \quad (21)$$

Since the step size is small enough that $\psi(\cdot) - \eta L_i(\cdot)$ is strictly convex for all i , the first term $D_{\psi-\eta L_i}(w_i, w_{i-1})$ is non-negative. The second term $\eta L_i(w_i)$ is non-negative because of the non-negativity of the loss. Finally, the last term $D_{L_i}(w, w_{i-1})$ is non-negative because $w_{i-1} \in \mathcal{B}$ for all i . Hence, all the three terms in the summand are non-negative, and because the sum is bounded, they should go to zero as $i \rightarrow \infty$. In particular,

$$D_{\psi-\eta L_i}(w_i, w_{i-1}) \rightarrow 0 \quad (22)$$

implies $w_i \rightarrow w_{i-1}$, i.e., convergence ($w_i \rightarrow w_\infty$), and further

$$\eta L_i(w_i) \rightarrow 0. \quad (23)$$

This implies that all the individual losses are going to zero, and since every data point is being revisited after some steps, all the data points are being fit. Therefore, $w_\infty \in \mathcal{W}$. \square

A.3 Closeness of the Final Point to the Regularized Solution

In this section, we show that with the additional Assumption 2 (which is equivalent to $f_i(\cdot)$ having bounded Hessian in \mathcal{B}), not only do the iterates remain in \mathcal{B} and converge to the set \mathcal{W} , but also they converge to a point which is very close to w^* (the closest solution to the initial point, in Bregman divergence). The proof is again based on our fundamental identity for SMD.

Assumption 2. Consider the region \mathcal{B} in Assumption 1. $f_i(\cdot)$ have bounded gradient and Hessian on the convex hull of \mathcal{B} , i.e., $\|\nabla f_i(w')\| \leq \gamma$, and $\alpha \leq \lambda_{\min}(H_{f_i}(w')) \leq \lambda_{\max}(H_{f_i}(w')) \leq \beta, i = 1, \dots, n$, for all $w' \in \text{conv } \mathcal{B}$.

Theorem 4. Define $w^* = \arg \min_{w \in \mathcal{W}} D_\psi(w, w_0)$. Under the assumptions of Theorem 3, and Assumption 2, the following holds.

1. $D_\psi(w_\infty, w_0) = D_\psi(w^*, w_0) + o(\epsilon)$
2. $D_\psi(w^*, w_\infty) = o(\epsilon)$

Proof of Theorem 4. Recall the identity of SMD from Lemma 6:

$$D_\psi(w, w_{i-1}) = D_\psi(w, w_i) + D_{\psi-\eta L_i}(w_i, w_{i-1}) + \eta L_i(w_i) + \eta D_{L_i}(w, w_{i-1}) \quad (9)$$

which holds for all $w \in \mathcal{W}$. Summing the identity for all $i \geq 1$, we have

$$D_\psi(w, w_0) = D_\psi(w, w_\infty) + \sum_{i=1}^{\infty} [D_{\psi-\eta L_i}(w_i, w_{i-1}) + \eta L_i(w_i) + \eta D_{L_i}(w, w_{i-1})]. \quad (24)$$

for all $w \in \mathcal{W}$. Note that the only terms in the right-hand side which depend on w are the first one $D_\psi(w, w_\infty)$ and the last one $\eta \sum_{i=1}^{\infty} D_{L_i}(w, w_{i-1})$. In what follows, We will argue that, within \mathcal{B} , the dependence on w in the last term is weak and therefore w_∞ is close to w^* .

To further spell out the dependence on w in the last term, let us expand $D_{L_i}(w, w_{i-1})$

$$D_{L_i}(w, w_{i-1}) = 0 - L_i(w_{i-1}) - \nabla L_i(w_{i-1})^T (w - w_{i-1}) \quad (25)$$

$$= -L_i(w_{i-1}) + \ell'(y_i - f_i(w_{i-1})) \nabla f_i(w_{i-1})^T (w - w_{i-1}) \quad (26)$$

for all $w \in \mathcal{W}$, where the first equality comes from the definition of $D_{L_i}(\cdot, \cdot)$ and the fact that $L_i(w) = 0$ for $w \in \mathcal{W}$. The second equality is from taking the derivative of $L_i(\cdot) = \ell(y_i - f_i(\cdot))$ and evaluating it at w_{i-1} .

By Taylor expansion of $f_i(w)$ around w_{i-1} and using Taylor's theorem (Lagrange's mean-value form), we have

$$f_i(w) = f_i(w_{i-1}) + \nabla f_i(w_{i-1})^T (w - w_{i-1}) + \frac{1}{2} (w - w_{i-1})^T H_{f_i}(\hat{w}_i) (w - w_{i-1}), \quad (27)$$

for some \hat{w}_i in the convex hull of w and w_{i-1} . Since $f_i(w) = y_i$ for all $w \in \mathcal{W}$, it follows that

$$\nabla f_i(w_{i-1})^T (w - w_{i-1}) = y_i - f_i(w_{i-1}) - \frac{1}{2} (w - w_{i-1})^T H_{f_i}(\hat{w}_i) (w - w_{i-1}), \quad (28)$$

for all $w \in \mathcal{W}$. Plugging this into (26), we have

$$D_{L_i}(w, w_{i-1}) = -L_i(w_{i-1}) + \ell'(y_i - f_i(w_{i-1})) \left(y_i - f_i(w_{i-1}) - \frac{1}{2} (w - w_{i-1})^T H_{f_i}(\hat{w}_i) (w - w_{i-1}) \right) \quad (29)$$

for all $w \in \mathcal{W}$. Finally, by plugging this back into the identity (24), we have

$$D_\psi(w, w_0) = D_\psi(w, w_\infty) + \sum_{i=1}^{\infty} \left[D_{\psi - \eta L_i}(w_i, w_{i-1}) + \eta L_i(w_i) - \eta L_i(w_{i-1}) + \eta \ell'(y_i - f_i(w_{i-1})) \left(y_i - f_i(w_{i-1}) - \frac{1}{2} (w - w_{i-1})^T H_{f_i}(\hat{w}_i) (w - w_{i-1}) \right) \right]. \quad (30)$$

for all $w \in \mathcal{W}$. Note that this can be expressed as

$$D_\psi(w, w_0) = D_\psi(w, w_\infty) + C - \sum_{i=1}^{\infty} \frac{1}{2} \eta \ell'(y_i - f_i(w_{i-1})) (w - w_{i-1})^T H_{f_i}(\hat{w}_i) (w - w_{i-1}), \quad (31)$$

for all $w \in \mathcal{W}$, where C does not depend on w :

$$C = \sum_{i=1}^{\infty} \left[D_{\psi - \eta L_i}(w_i, w_{i-1}) + \eta L_i(w_i) - \eta L_i(w_{i-1}) + \eta \ell'(y_i - f_i(w_{i-1})) (y_i - f_i(w_{i-1})) \right].$$

From Theorem 3, we know that $w_\infty \in \mathcal{W}$. Therefore, by plugging it into equation (31), and using the fact that $D_\psi(w_\infty, w_\infty) = 0$, we have

$$D_\psi(w_\infty, w_0) = C - \sum_{i=1}^{\infty} \frac{1}{2} \eta \ell'(y_i - f_i(w_{i-1})) (w_\infty - w_{i-1})^T H_{f_i}(w'_i) (w_\infty - w_{i-1}), \quad (32)$$

where w'_i is a point in the convex hull of w_∞ and w_{i-1} (and therefore also in $\text{conv } \mathcal{B}$), for all i . Similarly, by plugging w^* , which is also in \mathcal{W} , into (31), we have

$$D_\psi(w^*, w_0) = D_\psi(w^*, w_\infty) + C - \sum_{i=1}^{\infty} \frac{1}{2} \eta \ell'(y_i - f_i(w_{i-1})) (w^* - w_{i-1})^T H_{f_i}(w''_i) (w^* - w_{i-1}), \quad (33)$$

where w_i'' is a point in the convex hull of w^* and w_{i-1} (and therefore also in $\text{conv } \mathcal{B}$), for all i . Subtracting the last two equations from each other yields

$$D_\psi(w_\infty, w_0) - D_\psi(w^*, w_0) = -D_\psi(w^*, w_\infty) + \sum_{i=1}^{\infty} \frac{1}{2} \eta \ell'(y_i - f_i(w_{i-1})) \cdot [(w^* - w_{i-1})^T H_{f_i}(w_i'')(w^* - w_{i-1}) - (w_\infty - w_{i-1})^T H_{f_i}(w_i')(w_\infty - w_{i-1})]. \quad (34)$$

Note that since all w_i' and w_i'' are in $\text{conv } \mathcal{B}$, by Assumption 2, we have

$$\alpha \|w_\infty - w_{i-1}\|^2 \leq (w_\infty - w_{i-1})^T H_{f_i}(w_i')(w_\infty - w_{i-1}) \leq \beta \|w_\infty - w_{i-1}\|^2, \quad (35)$$

and

$$\alpha \|w^* - w_{i-1}\|^2 \leq (w^* - w_{i-1})^T H_{f_i}(w_i'')(w^* - w_{i-1}) \leq \beta \|w^* - w_{i-1}\|^2. \quad (36)$$

Further, again since all the iterates $\{w_i\}$ are in \mathcal{B} , it follows that $\|w_\infty - w_{i-1}\|^2 = O(\epsilon)$ and $\|w^* - w_{i-1}\|^2 = O(\epsilon)$. As a result the difference of the two terms, i.e., $[(w^* - w_{i-1})^T H_{f_i}(w_i'')(w^* - w_{i-1}) - (w_\infty - w_{i-1})^T H_{f_i}(w_i')(w_\infty - w_{i-1})]$, is also $O(\epsilon)$, and we have

$$D_\psi(w_\infty, w_0) - D_\psi(w^*, w_0) = -D_\psi(w^*, w_\infty) + \sum_{i=1}^{\infty} \eta \ell'(y_i - f_i(w_{i-1})) O(\epsilon). \quad (37)$$

Now note that $\ell'(y_i - f_i(w_{i-1})) = \ell'(f_i(w) - f_i(w_{i-1})) = \ell'(\nabla f_i(\tilde{w}_i)^T (w - w_{i-1}))$ for some $\tilde{w}_i \in \text{conv } \mathcal{B}$. Since $\|w - w_{i-1}\|^2 = O(\epsilon)$ for all i , and since $\ell(\cdot)$ is differentiable and $f_i(\cdot)$ have bounded derivatives, it follows that $\ell'(y_i - f_i(w_{i-1})) = o(\epsilon)$. Furthermore, the sum is bounded. This implies that $D_\psi(w_\infty, w_0) - D_\psi(w^*, w_0) = -D_\psi(w^*, w_\infty) + o(\epsilon)$, or equivalently

$$(D_\psi(w_\infty, w_0) - D_\psi(w^*, w_0)) + D_\psi(w^*, w_\infty) = o(\epsilon). \quad (38)$$

The term in parentheses $D_\psi(w_\infty, w_0) - D_\psi(w^*, w_0)$ is non-negative by definition of w^* . The second term $D_\psi(w^*, w_\infty)$ is non-negative by convexity of ψ . Since both terms are non-negative and their sum is $o(\epsilon)$, each one of them is at most $o(\epsilon)$, i.e.

$$\begin{cases} D_\psi(w_\infty, w_0) - D_\psi(w^*, w_0) = o(\epsilon) \\ D_\psi(w^*, w_\infty) = o(\epsilon) \end{cases} \quad (39)$$

which concludes the proof. \square

Corollary 5. *For the initialization $w_0 = \arg \min_{w \in \mathbb{R}^p} \psi(w)$, under the conditions of Theorem 4, $w^* = \arg \min_{w \in \mathcal{W}} \psi(w)$ and the following holds.*

1. $\psi(w_\infty) = \psi(w^*) + o(\epsilon)$
2. $D_\psi(w^*, w_\infty) = o(\epsilon)$

Proof of Corollary 5. The proof is a straightforward application of Theorem 4. Note that we have

$$D_\psi(w, w_0) = \psi(w) - \psi(w_0) - \nabla \psi(w_0)^T (w - w_0) \quad (40)$$

for all w . When $w_0 = \arg \min_{w \in \mathbb{R}^p} \psi(w)$, it follows that $\nabla \psi(w_0) = 0$, and

$$D_\psi(w, w_0) = \psi(w) - \psi(w_0). \quad (41)$$

In particular, by plugging in w_∞ and w^* , we have $D_\psi(w_\infty, w_0) = \psi(w_\infty) - \psi(w_0)$ and $D_\psi(w^*, w_0) = \psi(w^*) - \psi(w_0)$. Subtracting the two equations from each other yields

$$D_\psi(w_\infty, w_0) - D_\psi(w^*, w_0) = \psi(w_\infty) - \psi(w^*), \quad (42)$$

which along with the application of Theorem 4 concludes the proof. \square

A.4 Closeness to the Interpolating Set in Highly Overparameterized Models

As we mentioned earlier, it has been argued in a number of recent papers that for highly overparameterized models, any random initial point is, whp, close to the solution set \mathcal{W} [5, 25, 9, 2]. In the highly overparameterized regime, $p \gg n$, and so the dimension of the manifold \mathcal{W} , which is $p - n$, is very large. For simplicity, we outline an argument for the case of Euclidean distance, bearing in mind that a similar argument can be used for general Bregman divergence. Note that the distance of an arbitrarily chosen w_0 to \mathcal{W} is given by

$$\begin{aligned} \min_w \quad & \|w - w_0\|^2 \\ \text{s.t.} \quad & y = f(x, w) \end{aligned}$$

where $y = \text{vec}(y_i, i = 1, \dots, n)$ and $f(x, w) = \text{vec}(f(x_i, w), i = 1, \dots, n)$. This can be approximated by

$$\begin{aligned} \min_w \quad & \|w - w_0\|^2 \\ \text{s.t.} \quad & y \approx f(x, w_0) + \nabla f(x, w_0)^T (w - w_0) \end{aligned}$$

where $\nabla f(x, w_0)^T = \text{vec}(\nabla f(x_i, w)^T, i = 1, \dots, n)$ is the $n \times p$ Jacobian matrix. The latter optimization can be solved to yield

$$\|w_* - w_0\|^2 \approx (y - f(x, w_0))^T (\nabla f(x, w_0)^T \nabla f(x, w_0))^{-1} (y - f(x, w_0)) \quad (43)$$

Note that $\nabla f(x, w_0)^T \nabla f(x, w_0)$ is an $n \times n$ matrix consisting of the sum of p outer products. When the x_i are sufficiently random, and $p \gg n$, it is not unreasonable to assume that whp

$$\lambda_{\min} (\nabla f(x, w_0)^T \nabla f(x, w_0)) = \Omega(p),$$

from which we conclude

$$\|w_* - w_0\|^2 \approx \|y - f(x, w_0)\|^2 \cdot O\left(\frac{1}{p}\right) = O\left(\frac{n}{p}\right), \quad (44)$$

since $y - f(x, w_0)$ is n -dimensional. The above implies that w_0 is close to w_* and hence \mathcal{W} .

B More Details on the Experimental Results

In order to evaluate the claim, we run systematic experiments on some standard deep learning problems.

Datasets. We use the standard MNIST [23] and CIFAR-10 [20] datasets.

Architectures. For MNIST, we use a 4-layer convolutional neural network (CNN) with 2 convolution layers and 2 fully connected layers. The convolutional layers and the fully connected layers are picked wide enough to obtain 2×10^6 trainable parameters. Since MNIST dataset has 60,000 training samples, the number of parameters is significantly larger than the number of training data points, and the problem is highly overparameterized. For the CIFAR-10 dataset, we use the standard ResNet-18 [18] architecture without any modifications. CIFAR-10 has 50,000 training samples and with the total number of 11×10^6 parameters in ResNet-18, the problem is again highly overparameterized.

Loss Function. We use the cross-entropy loss as the loss function in our training. We train the models from different initializations, and with different mirror descents from each particular initialization, until we reach 100% training accuracy, i.e., until we hit \mathcal{W} .

Initialization. We randomly initialize the parameters of the networks around zero ($\mathcal{N}(0, 0.0001)$). We choose 6 independent initializations for the CNN, and 8 for ResNet-18, and for each initialization, we run the following 4 different SMD algorithms.

Algorithms. We use the mirror descent algorithms defined by the norm potential $\psi(w) = \frac{1}{q} \|w\|_q^q$ for the following four different norms: (a) ℓ_1 norm, i.e., $q = 1 + \epsilon$, (b) ℓ_2 norm, i.e., $q = 2$ (which is SGD), (c) ℓ_3 norm, i.e., $q = 3$, (d) ℓ_{10} norm, i.e., $q = 10$ (as a surrogate for ℓ_∞ norm). The update rule can be expressed as follows.

$$w_{i,j} = \left| |w_{i-1,j}|^{q-1} \text{sign}(w_{i-1,j}) - \eta \nabla L_i(w_{i-1})_j \right|^{\frac{1}{q-1}} \cdot \text{sign} \left(|w_{i-1,j}|^{q-1} \text{sign}(w_{i-1,j}) - \eta \nabla L_i(w_{i-1})_j \right), \quad (45)$$

where $w_{i-1,j}$ denotes the j -th element of the w_{i-1} vector.

We use a fixed step size η . The step size is chosen to obtain convergence to global minima.

B.1 MNIST Experiments

B.1.1 Closest Minimum for Different Mirror Descents with Fixed Initialization

We provide the distances from final points (global minima) obtained by different algorithms from the same initialization, measured in different Bregman divergences for MNIST classification task using a standard CNN. Note that in all tables the smallest element in each row is on the diagonal, which means the point achieved by each mirror has the smallest Bregman divergence to the initialization corresponding to that mirror, among all mirrors. Tables 3, 4, 5, 6, 7, 8 depict these results for 6 different initializations. The rows are the distance metrics used as the Bregman Divergences with specified potentials. The columns are the global minima obtained using specified SMD algorithms.

Table 3: MNIST Initial Point 1

	SMD 1-norm	SMD 2-norm (SGD)	SMD 3-norm	SMD 10-norm
1-norm BD	2.767	937.8	1.05×10^4	1.882×10^5
2-norm BD	301.6	58.61	261.3	2.118×10^4
3-norm BD	1720	37.45	7.143	2518
10-norm BD	7.453×10^8	773.4	0.2939	0.003545

Table 4: MNIST Initial Point 2

	SMD 1-norm	SMD 2-norm (SGD)	SMD 3-norm	SMD 10-norm
1-norm BD	2.78	945	1.37×10^4	2.01×10^5
2-norm BD	292	59.3	374	2.29×10^4
3-norm BD	1.51×10^3	38.6	11.6	2.71×10^3
10-norm BD	1.06×10^8	831	0.86	0.00321

Table 5: MNIST Initial Point 3

	SMD 1-norm	SMD 2-norm (SGD)	SMD 3-norm	SMD 10-norm
1-norm BD	3.02	968	1.06×10^4	1.9×10^5
2-norm BD	291	60.9	272	2.12×10^4
3-norm BD	1.49×10^3	39.1	7.82	2.49×10^3
10-norm BD	1.1×10^8	900	0.411	0.00318

Table 6: MNIST Initial Point 4

	SMD 1-norm	SMD 2-norm (SGD)	SMD 3-norm	SMD 10-norm
1-norm BD	2.78	1.21×10^3	1.08×10^4	1.92×10^5
2-norm BD	291	77.3	271	2.15×10^4
3-norm BD	1.48×10^3	49.7	7.56	2.52×10^3
10-norm BD	9.9×10^7	1.72×10^3	0.352	0.00296

Table 7: MNIST Initial Point 5

	SMD 1-norm	SMD 2-norm (SGD)	SMD 3-norm	SMD 10-norm
1-norm BD	2.79	958	1.08×10^4	2×10^5
2-norm BD	292	60.4	271	2.28×10^4
3-norm BD	1.49×10^3	39	7.52	2.69×10^3
10-norm BD	9.09×10^7	846	0.342	0.00309

Table 8: MNIST Initial Point 6

	SMD 1-norm	SMD 2-norm (SGD)	SMD 3-norm	SMD 10-norm
1-norm BD	2.96	930	1.08×10^4	1.9×10^5
2-norm BD	308	59	271	2.12×10^4
3-norm BD	1.63×10^3	38.6	7.46	2.47×10^3
10-norm BD	1.65×10^8	864	0.334	0.00295

B.1.2 Closest Minimum for Different Initalizations with Fixed Mirror

We provide the pairwise distances between different initial points and the final points (global minima) obtained by using fixed SMD algorithms in MNIST dataset using a standard CNN. Note that the smallest element in each row is on the diagonal, which means the closest final point to each initialization, among all the final points, is the one corresponding to that point. Tables 9, 10, 11 and 12 depict these results for 4 different SMD algorithms. The rows are the initial points and the columns are the final points corresponding to each initialization.

Table 9: MNIST 1-norm Bregman Divergence Between the Initial Points and the Final Points obtained by SMD 1-norm

	Final 1	Final 2	Final 3	Final 4	Final 5	Final 6
Initial Point 1	2.7671	20311	20266	20331	20340	20282
Initial Point 2	20332	2.7774	20281	20299	20312	20323
Initial Point 3	20319	20312	3.018	20344	20309	20322
Initial Point 4	20339	20279	20310	2.781	20321	20297
Initial Point 5	20347	20317	20273	20316	2.7902	20311
Initial Point 6	20344	20323	20340	20318	20321	2.964

Table 10: MNIST 2-norm Bregman Divergence Between the Initial Points and the Final Points obtained by SMD 2-norm (SGD)

	Final 1	Final 2	Final 3	Final 4	Final 5	Final 6
Initial Point 1	58.608	670.75	667.03	684.18	671.36	667.84
Initial Point 2	669.84	59.315	669.16	682.04	669.45	669.98
Initial Point 3	666.35	670.22	60.858	683.44	667.57	669.99
Initial Point 4	669.71	668.86	671.19	77.275	670.33	669.7
Initial Point 5	671.1	669.12	668.45	683.61	60.39	666.04
Initial Point 6	669.46	670.92	671.59	684.32	667.37	59.043

Table 11: MNIST 3-norm Bregman Divergence Between the Initial Points and the Final Points obtained by SMD 3-norm

	Final 1	Final 2	Final 3	Final 4	Final 5	Final 6
Initial Point 1	7.143	35.302	32.077	32.659	32.648	32.309
Initial Point 2	32.507	11.578	32.256	32.325	32.225	32.46
Initial Point 3	31.594	34.643	7.8239	32.521	31.58	32.519
Initial Point 4	32.303	34.811	32.937	7.5589	32.617	32.284
Initial Point 5	32.673	34.678	32.071	32.738	7.5188	31.558
Initial Point 6	32.116	34.731	32.376	32.431	31.699	7.4593

Table 12: MNIST 10-norm Bregman Divergence Between the Initial Points and the Final Points obtained by SMD 10-norm

	Final 1	Final 2	Final 3	Final 4	Final 5	Final 6
Initial Point 1	0.00354	0.37	0.403	0.286	0.421	0.408
Initial Point 2	0.33	0.00321	0.369	0.383	0.415	0.422
Initial Point 3	0.347	0.318	0.00318	0.401	0.312	0.406
Initial Point 4	0.282	0.38	0.458	0.00296	0.491	0.376
Initial Point 5	0.405	0.418	0.354	0.484	0.00309	0.48
Initial Point 6	0.403	0.353	0.422	0.331	0.503	0.00295

B.1.3 Closest Minimum for Different Initalizations and Different Mirrors

Now we assess the pairwise distances between different initial points and final points (global minima) obtained by all different initalizations and all different mirrors (Table 8). The smallest element in each row is exactly the final point obtained by that mirror from that initialization, among all the mirrors and all the initial points.

	F1 SMD 1	F2 SMD 1	F3 SMD 1	F4 SMD 1	F5 SMD 1	F6 SMD 1	F7 SMD 1	F8 SMD 1	F9 SMD 1	F10 SMD 1	F11 SMD 1	F12 SMD 1	F13 SMD 1	F14 SMD 1	F15 SMD 1	F16 SMD 1	F17 SMD 1	F18 SMD 1	F19 SMD 1	F20 SMD 1	F21 SMD 1	F22 SMD 1	F23 SMD 1	F24 SMD 1	F25 SMD 1	F26 SMD 1	F27 SMD 1	F28 SMD 1	F29 SMD 1	F30 SMD 1	F31 SMD 1	F32 SMD 1	F33 SMD 1	F34 SMD 1	F35 SMD 1	F36 SMD 1	F37 SMD 1	F38 SMD 1	F39 SMD 1	F40 SMD 1	F41 SMD 1	F42 SMD 1	F43 SMD 1	F44 SMD 1	F45 SMD 1	F46 SMD 1	F47 SMD 1	F48 SMD 1	F49 SMD 1	F50 SMD 1	F51 SMD 1	F52 SMD 1	F53 SMD 1	F54 SMD 1	F55 SMD 1	F56 SMD 1	F57 SMD 1	F58 SMD 1	F59 SMD 1	F60 SMD 1	F61 SMD 1	F62 SMD 1	F63 SMD 1	F64 SMD 1	F65 SMD 1	F66 SMD 1	F67 SMD 1	F68 SMD 1	F69 SMD 1	F70 SMD 1	F71 SMD 1	F72 SMD 1	F73 SMD 1	F74 SMD 1	F75 SMD 1	F76 SMD 1	F77 SMD 1	F78 SMD 1	F79 SMD 1	F80 SMD 1	F81 SMD 1	F82 SMD 1	F83 SMD 1	F84 SMD 1	F85 SMD 1	F86 SMD 1	F87 SMD 1	F88 SMD 1	F89 SMD 1	F90 SMD 1	F91 SMD 1	F92 SMD 1	F93 SMD 1	F94 SMD 1	F95 SMD 1	F96 SMD 1	F97 SMD 1	F98 SMD 1	F99 SMD 1	F100 SMD 1																																																																																																																																																																																																																																																																																																																																																																																																																																																																																																																																																																																																																																																																																																																																																																																			
11 1-norm BD	2.767105	20310.58	20322.66	20330.6	20340.2	20349.8	20359.4	20369.0	20378.6	20388.2	20397.8	20407.4	20417.0	20426.6	20436.2	20445.8	20455.4	20465.0	20474.6	20484.2	20493.8	20503.4	20513.0	20522.6	20532.2	20541.8	20551.4	20561.0	20570.6	20580.2	20589.8	20599.4	20609.0	20618.6	20628.2	20637.8	20647.4	20657.0	20666.6	20676.2	20685.8	20695.4	20705.0	20714.6	20724.2	20733.8	20743.4	20753.0	20762.6	20772.2	20781.8	20791.4	20801.0	20810.6	20820.2	20829.8	20839.4	20849.0	20858.6	20868.2	20877.8	20887.4	20897.0	20906.6	20916.2	20925.8	20935.4	20945.0	20954.6	20964.2	20973.8	20983.4	20993.0	21002.6	21012.2	21021.8	21031.4	21041.0	21050.6	21060.2	21069.8	21079.4	21089.0	21098.6	21108.2	21117.8	21127.4	21137.0	21146.6	21156.2	21165.8	21175.4	21185.0	21194.6	21204.2	21213.8	21223.4	21233.0	21242.6	21252.2	21261.8	21271.4	21281.0	21290.6	21300.2	21309.8	21319.4	21329.0	21338.6	21348.2	21357.8	21367.4	21377.0	21386.6	21396.2	21405.8	21415.4	21425.0	21434.6	21444.2	21453.8	21463.4	21473.0	21482.6	21492.2	21501.8	21511.4	21521.0	21530.6	21540.2	21549.8	21559.4	21569.0	21578.6	21588.2	21597.8	21607.4	21617.0	21626.6	21636.2	21645.8	21655.4	21665.0	21674.6	21684.2	21693.8	21703.4	21713.0	21722.6	21732.2	21741.8	21751.4	21761.0	21770.6	21780.2	21789.8	21799.4	21809.0	21818.6	21828.2	21837.8	21847.4	21857.0	21866.6	21876.2	21885.8	21895.4	21905.0	21914.6	21924.2	21933.8	21943.4	21953.0	21962.6	21972.2	21981.8	21991.4	22001.0	22010.6	22020.2	22029.8	22039.4	22049.0	22058.6	22068.2	22077.8	22087.4	22097.0	22106.6	22116.2	22125.8	22135.4	22145.0	22154.6	22164.2	22173.8	22183.4	22193.0	22202.6	22212.2	22221.8	22231.4	22241.0	22250.6	22260.2	22269.8	22279.4	22289.0	22298.6	22308.2	22317.8	22327.4	22337.0	22346.6	22356.2	22365.8	22375.4	22385.0	22394.6	22404.2	22413.8	22423.4	22433.0	22442.6	22452.2	22461.8	22471.4	22481.0	22490.6	22500.2	22509.8	22519.4	22529.0	22538.6	22548.2	22557.8	22567.4	22577.0	22586.6	22596.2	22605.8	22615.4	22625.0	22634.6	22644.2	22653.8	22663.4	22673.0	22682.6	22692.2	22701.8	22711.4	22721.0	22730.6	22740.2	22749.8	22759.4	22769.0	22778.6	22788.2	22797.8	22807.4	22817.0	22826.6	22836.2	22845.8	22855.4	22865.0	22874.6	22884.2	22893.8	22903.4	22913.0	22922.6	22932.2	22941.8	22951.4	22961.0	22970.6	22980.2	22989.8	22999.4	23009.0	23018.6	23028.2	23037.8	23047.4	23057.0	23066.6	23076.2	23085.8	23095.4	23105.0	23114.6	23124.2	23133.8	23143.4	23153.0	23162.6	23172.2	23181.8	23191.4	23201.0	23210.6	23220.2	23229.8	23239.4	23249.0	23258.6	23268.2	23277.8	23287.4	23297.0	23306.6	23316.2	23325.8	23335.4	23345.0	23354.6	23364.2	23373.8	23383.4	23393.0	23402.6	23412.2	23421.8	23431.4	23441.0	23450.6	23460.2	23469.8	23479.4	23489.0	23498.6	23508.2	23517.8	23527.4	23537.0	23546.6	23556.2	23565.8	23575.4	23585.0	23594.6	23604.2	23613.8	23623.4	23633.0	23642.6	23652.2	23661.8	23671.4	23681.0	23690.6	23700.2	23709.8	23719.4	23729.0	23738.6	23748.2	23757.8	23767.4	23777.0	23786.6	23796.2	23805.8	23815.4	23825.0	23834.6	23844.2	23853.8	23863.4	23873.0	23882.6	23892.2	23901.8	23911.4	23921.0	23930.6	23940.2	23949.8	23959.4	23969.0	23978.6	23988.2	23997.8	24007.4	24017.0	24026.6	24036.2	24045.8	24055.4	24065.0	24074.6	24084.2	24093.8	24103.4	24113.0	24122.6	24132.2	24141.8	24151.4	24161.0	24170.6	24180.2	24189.8	24199.4	24209.0	24218.6	24228.2	24237.8	24247.4	24257.0	24266.6	24276.2	24285.8	24295.4	24305.0	24314.6	24324.2	24333.8	24343.4	24353.0	24362.6	24372.2	24381.8	24391.4	24401.0	24410.6	24420.2	24429.8	24439.4	24449.0	24458.6	24468.2	24477.8	24487.4	24497.0	24506.6	24516.2	24525.8	24535.4	24545.0	24554.6	24564.2	24573.8	24583.4	24593.0	24602.6	24612.2	24621.8	24631.4	24641.0	24650.6	24660.2	24669.8	24679.4	24689.0	24698.6	24708.2	24717.8	24727.4	24737.0	24746.6	24756.2	24765.8	24775.4	24785.0	24794.6	24804.2	24813.8	24823.4	24833.0	24842.6	24852.2	24861.8	24871.4	24881.0	24890.6	24900.2	24909.8	24919.4	24929.0	24938.6	24948.2	24957.8	24967.4	24977.0	24986.6	24996.2	25005.8	25015.4	25025.0	25034.6	25044.2	25053.8	25063.4	25073.0	25082.6	25092.2	25101.8	25111.4	25121.0	25130.6	25140.2	25149.8	25159.4	25169.0	25178.6	25188.2	25197.8	25207.4	25217.0	25226.6	25236.2	25245.8	25255.4	25265.0	25274.6	25284.2	25293.8	25303.4	25313.0	25322.6	25332.2	25341.8	25351.4	25361.0	25370.6	25380.2	25389.8	25399.4	25409.0	25418.6	25428.2	25437.8	25447.4	25457.0	25466.6	25476.2	25485.8	25495.4	25505.0	25514.6	25524.2	25533.8	25543.4	25553.0	25562.6	25572.2	25581.8	25591.4	25601.0	25610.6	25620.2	25629.8	25639.4	25649.0	25658.6	25668.2	25677.8	25687.4	25697.0	25706.6	25716.2	25725.8	25735.4	25745.0	25754.6	25764.2	25773.8	25783.4	25793.0	25802.6	25812.2	25821.8	25831.4	25841.0	25850.6	25860.2	25869.8	25879.4	25889.0	25898.6	25908.2	25917.8	25927.4	25937.0	25946.6	25956.2	25965.8	25975.4	25985.0	25994.6	26004.2	26013.8	26023.4	26033.0	26042.6	26052.2	26061.8	26071.4	26081.0	26090.6	26100.2	26109.8	26119.4	26129.0	26138.6	26148.2	26157.8	26167.4	26177.0	26186.6	26196.2	26205.8	26215.4	26225.0	26234.6	26244.2	26253.8	26263.4	26273.0	26282.6	26292.2	26301.8	26311.4	26321.0	26330.6	26340.2	26349.8	26359.4	26369.0	26378.6	26388.2	26397.8	26407.4	26417.0	26426.6	26436.2	26445.8	26455.4	26465.0	26474.6	26484.2	26493.8	26503.4	26513.0	26522.6	26532.2	26541.8	26551.4	26561.0	26570.6	26580.2	26589.8	26599.4	26609.0	26618.6	26628.2	26637.8	26647.4	26657.0	26666.6	26676.2	26685.8	26695.4	26705.0	26714.6	26724.2	26733.8	26743.4	26753.0	26762.6	26772.2	26781.8	26791.4	26801.0	26810.6	26820.2	26829.8	26839.4	26849.0	26858.6	26868.2	26877.8	26887.4	26897.0	26906.6	26916.2	26925.8	26935.4	26945.0	26954.6	26964.2	26973.8	26983.4	26993.0	27002.6	27012.2	27021.8	27031.4	27041.0	27050.6	27060.2	27069.8	27079.4	27089.0	27098.6	27108.2	27117.8	27127.4	27137.0	27146.6	27156.2	27165.8	27175.4	27185.0	27194.6	27204.2	27213.8	27223.4	27233.0	27242.6	27252.2	27261.8	27271.4	27281.0	27290.6	27300.2	27309.8	27319.4	27329.0	27338.6	27348.2	27357.8	27367.4	27377.0	27386.6	27396.2	27405.8	27415.4	27425.0	27434.6	27444.2	27453.8	27463.4	27473.0	27482.6	27492.2	27501.8	27511.4	27521.0	27530.6	27540.2	27549.8	27559.4	27569.0	27578.6	27588.2	27597.8	27607.4	27617.0	27626.6	27636.2	27645.8	27655.4	27665.0	27674.6	27684.2	27693.8	27703.4	27713.0	27722.6	27732.2	27741.8	27751.4	27761.0	27770.6	27780.2	27789.8	27799.4	27809.0	27818.6	27828.2	27837.8	27847.4	27857.0	27866.6	27876.2	27885.8	27895.4	27905.0	27914.6	27924.2	27933.8	27943.4	27953.0	27962.6	27972.2	27981.8	27991.4	28001.0	28010.6	28020.2	28029.8	28039.4	28049.0	28058.6	28068.2	28077.8	28087.4	28097.0	28106.6	28116.2	28125.8	28135.4	28145.0	28154.6	28164.2	28173.8	28183.4	28193.0	28202.6	28212.2	28221.8	28231.4	28241.0	28250.6	28260.2	28269.8	28279.4	28289.0	28298.6	28308.2	28317.8	28327.4	28337.0	28346.6	28356.2	28365.8	28375.4	28385.0	28394.6	28404.2	28413.8	28423.4	28433.0	28442.6	28452.2	28461.8	28471.4	28481.0	28490.6	28500.2

B.2 CIFAR-10 Experiments

B.2.1 Closest Minimum for Different Mirror Descents with Fixed Initialization

We provide the distances from final points (global minima) obtained by different algorithms from the same initialization, measured in different Bregman divergences for CIFAR-10 classification task using ResNet-18. Note that in all tables the smallest element in each row is on the diagonal, which means the point achieved by each mirror has the smallest Bregman divergence to the initialization corresponding to that mirror, among all mirrors. Tables 13, 14, 15, 16, 17, 18, 19, 20 depict these results for 8 different initializations. The rows are the distance metrics used as the Bregman Divergences with specified potentials. The columns are the global minima obtained using specified SMD algorithms.

Table 13: CIFAR-10 Initial Point 1

	SMD 1-norm	SMD 2-norm (SGD)	SMD 3-norm	SMD 10-norm
1-norm BD	189	9.58×10^3	4.19×10^4	2.34×10^5
2-norm BD	3.12×10^3	597	1.28×10^3	6.92×10^3
3-norm BD	4.31×10^4	119	55.8	1.87×10^2
10-norm BD	1.35×10^{14}	869	6.34×10^{-5}	2.64×10^{-8}

Table 14: CIFAR-10 Initial Point 2

	SMD 1-norm	SMD 2-norm (SGD)	SMD 3-norm	SMD 10-norm
1-norm BD	275	9.86×10^3	4.09×10^4	2.38×10^5
2-norm BD	4.89×10^3	607	1.23×10^3	7.03×10^3
3-norm BD	9.21×10^4	104	53.5	1.88×10^2
10-norm BD	1.17×10^{15}	225	0.000102	2.65×10^{-8}

Table 15: CIFAR-10 Initial Point 3

	SMD 1-norm	SMD 2-norm (SGD)	SMD 3-norm	SMD 10-norm
1-norm BD	141	9.19×10^3	4.1×10^4	2.34×10^5
2-norm BD	3.15×10^3	562	1.24×10^3	6.89×10^3
3-norm BD	4.31×10^4	107	53.5	1.85×10^2
10-norm BD	6.83×10^{13}	972	7.91×10^{-5}	2.72×10^{-8}

Table 16: CIFAR-10 Initial Point 4

	SMD 1-norm	SMD 2-norm (SGD)	SMD 3-norm	SMD 10-norm
1-norm BD	255	9.77×10^3	4.18×10^4	2.36×10^5
2-norm BD	3.64×10^3	594	1.26×10^3	6.96×10^3
3-norm BD	5.5×10^4	116	54	1.87×10^2
10-norm BD	3.74×10^{14}	640	5.33×10^{-5}	2.67×10^{-8}

Table 17: CIFAR-10 Initial Point 5

	SMD 1-norm	SMD 2-norm (SGD)	SMD 3-norm	SMD 10-norm
1-norm BD	113	9.48×10^3	4.15×10^4	2.32×10^5
2-norm BD	2.95×10^3	572	1.27×10^3	6.85×10^3
3-norm BD	3.68×10^4	109	56.2	1.84×10^2
10-norm BD	2.97×10^{13}	151	5.74×10^{-5}	2.61×10^{-8}

Table 18: CIFAR-10 Initial Point 6

	SMD 1-norm	SMD 2-norm (SGD)	SMD 3-norm	SMD 10-norm
1-norm BD	128	9.25×10^3	4.25×10^4	2.34×10^5
2-norm BD	2.71×10^3	558	1.29×10^3	6.89×10^3
3-norm BD	3.34×10^4	104	55.3	1.85×10^2
10-norm BD	2.61×10^{13}	612	4.74×10^{-5}	2.62×10^{-8}

Table 19: CIFAR-10 Initial Point 7

	SMD 1-norm	SMD 2-norm (SGD)	SMD 3-norm	SMD 10-norm
1-norm BD	223	9.76×10^3	4.38×10^4	2.27×10^5
2-norm BD	2.41×10^3	599	1.37×10^3	6.65×10^3
3-norm BD	2.3×10^4	116	61	1.78×10^2
10-norm BD	4.22×10^{12}	679	6.42×10^{-5}	2.55×10^{-8}

Table 20: CIFAR-10 Initial Point 8

	SMD 1-norm	SMD 2-norm (SGD)	SMD 3-norm	SMD 10-norm
1-norm BD	145	9.37×10^3	4.17×10^4	2.36×10^5
2-norm BD	2.48×10^3	576	1.26×10^3	6.99×10^3
3-norm BD	2.85×10^4	108	54.5	1.89×10^2
10-norm BD	1.81×10^{13}	1.22×10^3	5.2×10^{-5}	2.64×10^{-8}

B.2.2 Closest Minimum for Different Initalizations with Fixed Mirror

We provide the pairwise distances between different initial points and the final points (global minima) obtained by using fixed SMD algorithms in CIFAR-10 dataset using ResNet-18. Note that the smallest element in each row is on the diagonal, which means the closest final point to each initialization, among all the final points, is the one corresponding to that point. Tables 21, 22, 23, 24 depict these results for 4 different SMD algorithms. The rows are the initial points and the columns are the final points corresponding to each initialization.

Table 21: CIFAR-10 1-norm Bregman Divergence Between the Initial Points and the Final Points obtained by SMD 1-norm

	Final 1	Final 2	Final 3	Final 4	Final 5	Final 6	Final 7	Final 8
Initial 1	1.9×10^2	8.1×10^4	8.1×10^4	8.4×10^4	8×10^4	8.2×10^4	7.8×10^4	7.8×10^4
Initial 2	8.1×10^4	2.7×10^2	8.1×10^4	8.3×10^4	8×10^4	8.2×10^4	7.8×10^4	7.9×10^4
Initial 3	8.1×10^4	8.1×10^4	1.4×10^2	8.4×10^4	8×10^4	8.1×10^4	7.8×10^4	7.8×10^4
Initial 4	8.1×10^4	8.1×10^4	8.1×10^4	2.5×10^2	8×10^4	8.2×10^4	7.8×10^4	7.9×10^4
Initial 5	8.1×10^4	8.1×10^4	8.1×10^4	8.3×10^4	1.1×10^2	8.1×10^4	7.8×10^4	7.8×10^4
Initial 6	8.1×10^4	8.1×10^4	8.1×10^4	8.4×10^4	8×10^4	1.3×10^2	7.8×10^4	7.8×10^4
Initial 7	8.1×10^4	8.1×10^4	8.1×10^4	8.4×10^4	8×10^4	8.1×10^4	2.2×10^2	7.8×10^4
Initial 8	8.1×10^4	8.1×10^4	8.1×10^4	8.4×10^4	7.9×10^4	8.1×10^4	7.8×10^4	1.5×10^2

Table 22: CIFAR-10 2-norm Bregman Divergence Between the Initial Points and the Final Points obtained by SMD 2-norm (SGD)

	Final 1	Final 2	Final 3	Final 4	Final 5	Final 6	Final 7	Final 8
Initial 1	6×10^2	2.9×10^3	2.8×10^3					
Initial 2	2.8×10^3	6.1×10^2	2.8×10^3					
Initial 3	2.8×10^3	2.9×10^3	5.6×10^2	2.8×10^3				
Initial 4	2.8×10^3	2.9×10^3	2.8×10^3	5.9×10^2	2.8×10^3	2.8×10^3	2.8×10^3	2.8×10^3
Initial 5	2.8×10^3	2.9×10^3	2.8×10^3	2.8×10^3	5.7×10^2	2.8×10^3	2.8×10^3	2.8×10^3
Initial 6	2.8×10^3	2.9×10^3	2.8×10^3	2.8×10^3	2.8×10^3	5.6×10^2	2.8×10^3	2.8×10^3
Initial 7	2.8×10^3	2.9×10^3	2.8×10^3	2.8×10^3	2.8×10^3	2.8×10^3	6×10^2	2.8×10^3
Initial 8	2.8×10^3	2.9×10^3	2.8×10^3	5.8×10^2				

Table 23: CIFAR-10 3-norm Bregman Divergence Between the Initial Points and the Final Points obtained by SMD 3-norm

	Final 1	Final 2	Final 3	Final 4	Final 5	Final 6	Final 7	Final 8
Initial 1	55.844	103.47	103.61	104.05	106.2	105.32	110.88	104.56
Initial 2	105.87	53.455	103.68	104.04	106.31	105.34	110.93	104.58
Initial 3	105.89	103.59	53.527	104.09	106.29	105.35	110.99	104.55
Initial 4	105.83	103.54	103.64	53.978	106.23	105.3	110.87	104.54
Initial 5	105.82	103.55	103.64	104	56.161	105.34	110.88	104.55
Initial 6	105.91	103.6	103.66	104.1	106.28	55.316	110.94	104.55
Initial 7	105.87	103.51	103.67	103.98	106.26	105.25	61.045	104.5
Initial 8	105.77	103.54	103.59	104.04	106.25	105.28	110.88	54.509

Table 24: CIFAR-10 10-norm Bregman Divergence Between the Initial Points and the Final Points obtained by SMD 10-norm

	Final 1	Final 2	Final 3	Final 4	Final 5	Final 6	Final 7	Final 8
Initial 1	2.64×10^{-8}	2.89×10^{-8}	2.99×10^{-8}	2.81×10^{-8}	2.85×10^{-8}	2.82×10^{-8}	2.66×10^{-8}	2.82×10^{-8}
Initial 2	2.79×10^{-8}	2.65×10^{-8}	2.83×10^{-8}	2.83×10^{-8}	2.71×10^{-8}	2.74×10^{-8}	2.69×10^{-8}	2.88×10^{-8}
Initial 3	2.89×10^{-8}	2.87×10^{-8}	2.72×10^{-8}	2.94×10^{-8}	2.84×10^{-8}	2.89×10^{-8}	2.78×10^{-8}	2.94×10^{-8}
Initial 4	2.79×10^{-8}	2.86×10^{-8}	2.92×10^{-8}	2.67×10^{-8}	2.84×10^{-8}	2.81×10^{-8}	2.69×10^{-8}	2.85×10^{-8}
Initial 5	2.76×10^{-8}	2.88×10^{-8}	2.95×10^{-8}	2.93×10^{-8}	2.61×10^{-8}	2.73×10^{-8}	2.66×10^{-8}	2.83×10^{-8}
Initial 6	2.80×10^{-8}	2.76×10^{-8}	2.93×10^{-8}	2.79×10^{-8}	2.76×10^{-8}	2.62×10^{-8}	2.71×10^{-8}	2.85×10^{-8}
Initial 7	2.73×10^{-8}	2.76×10^{-8}	2.82×10^{-8}	2.79×10^{-8}	2.71×10^{-8}	2.77×10^{-8}	2.55×10^{-8}	2.83×10^{-8}
Initial 8	2.73×10^{-8}	2.79×10^{-8}	2.85×10^{-8}	2.78×10^{-8}	2.75×10^{-8}	2.74×10^{-8}	2.73×10^{-8}	2.64×10^{-8}

B.2.3 Closest Minimum for Different Initalizations and Different Mirrors

Now we assess the pairwise distances between different initial points and final points (global minima) obtained by all different initalizations and all different mirrors (Table 8). The smallest element in each row is exactly the final point obtained by that mirror from that initialization, among all the mirrors and all the initial points.

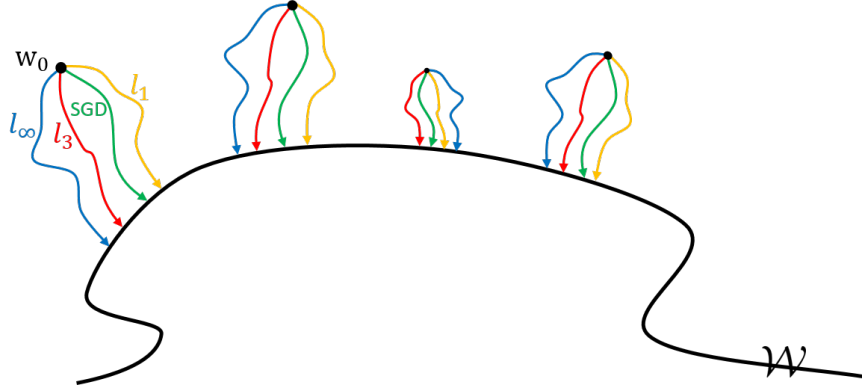


Figure 10: An illustration of the experimental results. For each initialization w_0 , we ran different SMD algorithms until convergence to a point on the set \mathcal{W} (zero training error). We then measured all the pairwise distances from different w_∞ to different w_0 , in different Bregman divergences. The closest point (among all initializations and all mirrors) to any particular initialization w_0 in Bregman divergence with potential $\psi(\cdot) = \|\cdot\|_q^q$ is exactly the point obtained by running SMD with potential $\|\cdot\|_q^q$ from w_0 .

B.3 Distribution of the Final Weights of the Network

One may be curious to see how the final weights obtained by these different mirrors look like, and whether, for example, mirror descent corresponding to the ℓ_1 -norm potential induces sparsity. We examine the distribution of the weights in the network for these algorithms starting from the same initialization. Fig. 11 shows the histogram of the initial weights, which follows a half-normal distribution. Figs. 12 (a), (b), (c), (d) show the histogram of the weights for ℓ_1 -SMD, ℓ_2 -SMD (SGD), ℓ_3 -SMD, and ℓ_{10} -SMD, respectively. Note that each of the four histograms corresponds to an 11×10^6 -dimensional weight vector that perfectly interpolates the data. Even though, perhaps as expected, the weights remain quite small, the histograms are drastically different. The histogram of the ℓ_1 -SMD has more weights at and close to zero, which again confirms that it induces sparsity. However, as will be shown in the next section, this is not necessarily good for generalization (in fact, it turns out that ℓ_{10} -SMD has a much better generalization). The histogram of the ℓ_2 -SMD (SGD) looks almost identical to the histogram of the initialization, whereas the ℓ_3 and ℓ_{10} histograms are shifted to the right, so much so that almost all weights in the ℓ_{10} solution are non-zero and in the range of 0.005 to 0.04. For comparison, all the distributions are shown together in Fig. 12(e).

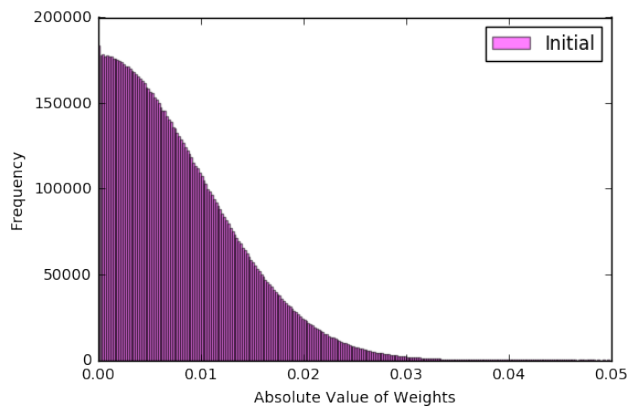


Figure 11: Histogram of the absolute value of the initial weights in the network (half-normal distribution)

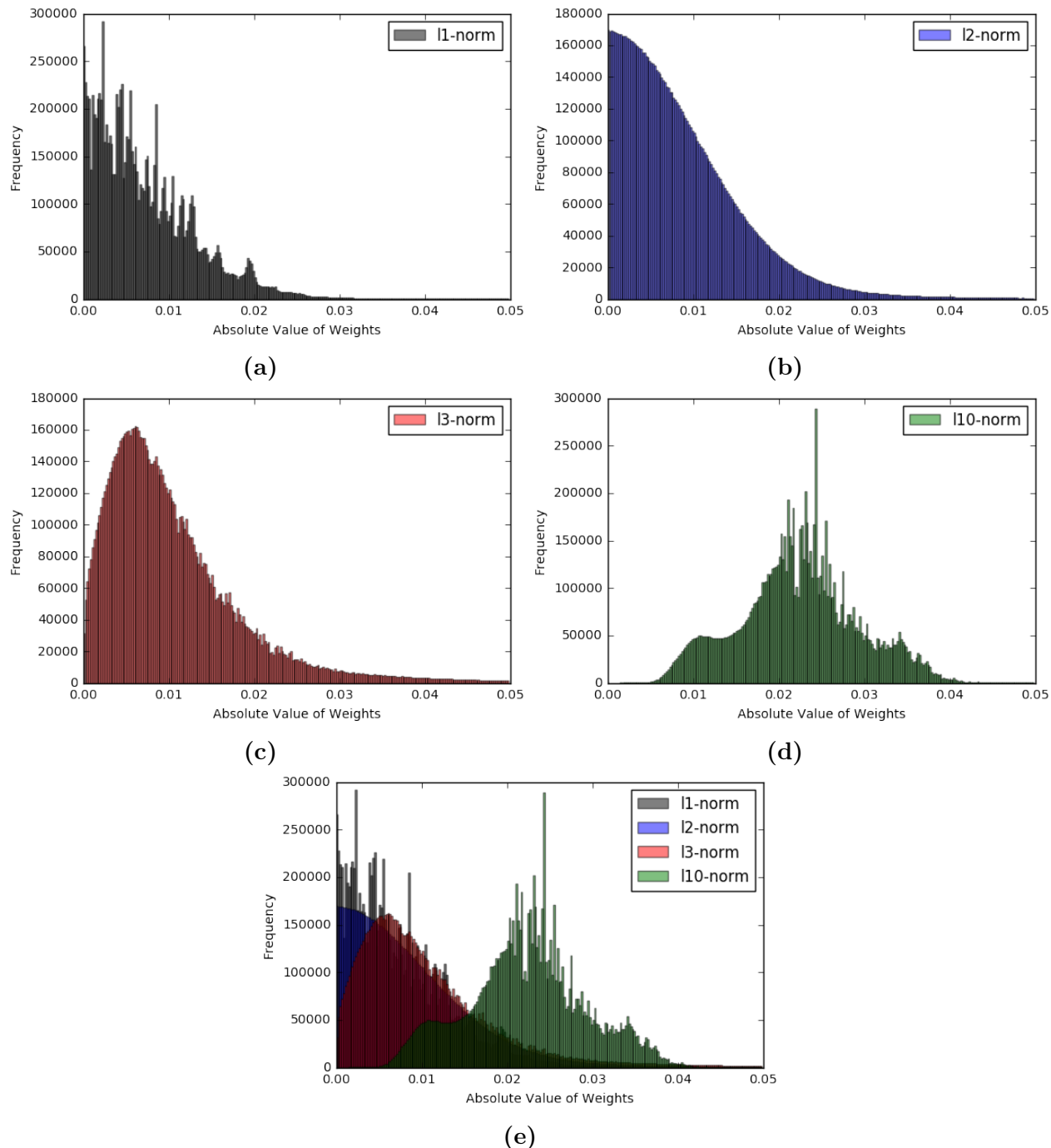


Figure 12: Histogram of the absolute value of the final weights in the network for different SMD algorithms: (a) l_1 -SMD, (b) l_2 -SMD (SGD), (c) l_3 -SMD, (d) l_{10} -SMD. Note that each of the four histograms corresponds to an 11×10^6 -dimensional weight vector that perfectly interpolates the data. Even though the weights remain quite small, the histograms are drastically different. l_1 -SMD induces sparsity on the weights, as expected. SGD does not seem to change the distribution of the weights significantly. l_3 -SMD starts to reduce the sparsity, and l_{10} shifts the distribution of the weights significantly, so much so that almost all the weights are non-zero.

B.4 Generalization Errors of Different Mirrors/Regularizers

In this section, we compare the performance of the SMD algorithms discussed before on the test set. This is important for understanding the effect of different regularizers on the generalization of deep networks.

For MNIST, perhaps not surprisingly, all the four SMD algorithms achieve around 99% or higher accuracy. For CIFAR-10, however, there is a significant difference between the test errors of different mirrors/regularizers on the same architecture. Fig. 13 shows the test accuracies of different algorithms with eight random initializations around zero, as discussed before. Counter-intuitively, ℓ_{10} performs consistently best, while ℓ_1 performs consistently worse. We should reiterate that the loss function is exactly the same in all these experiments, and all of them have been trained to fit the training set perfectly (zero training error). Therefore, the difference in generalization errors is purely the effect of implicit regularization by different algorithms. This result suggests the importance of a comprehensive study of the role of regularization, and the choice of the best regularizer, to improve the generalization performance of deep neural networks.

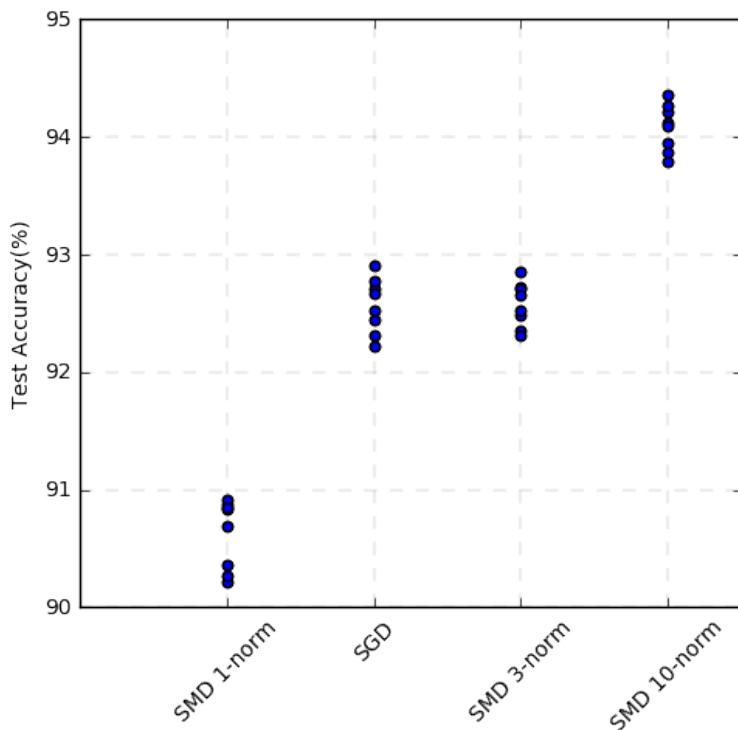


Figure 13: Generalization performance of different SMD algorithms on the CIFAR-10 dataset using ResNet-18. ℓ_{10} performs consistently better, while ℓ_1 performs consistently worse.